

UNIVERSITY OF OKLAHOMA

GRADUATE COLLEGE

VAPOR-PHASE ADSORPTIVE SEPARATION OF BIO-OIL COMPONENTS

USING ACTIVATED CARBON

A THESIS

SUBMITTED TO THE GRADUATE FACULTY

in partial fulfillment of the requirements for the

Degree of

MASTER OF SCIENCE

By

CHARLES JAKOB ALEXANDER CRUM

Norman, Oklahoma

2018

VAPOR-PHASE ADSORPTIVE SEPARATION OF BIO-OIL COMPONENTS  
USING ACTIVATED CARBON

A THESIS APPROVED FOR THE  
SCHOOL OF CHEMICAL, BIOLOGICAL AND MATERIALS ENGINEERING

BY

Dr. Lance Lobban, Chair

Dr. Steven Crossley

Dr. Daniel Resasco



## **Acknowledgements**

My thanks to the faculty of the University of Oklahoma School of Chemical, Biological, and Materials Engineering, especially Dr. Lance Lobban, for their advice, guidance, and support throughout this project and throughout my education.

My thanks to my family, for encouraging me to pursue whatever I was capable of, and for giving me the tools I needed to accomplish my goals, whichever goals I chose.

My thanks to all my friends, for helping me to stay on track and for lending advice, encouragement, and yes, even disapproval, when I needed to hear it the most.

And of course, my thanks to Kaitlin for her unconditional love and support.

## Table of Contents

Acknowledgements.....	iv
List of Tables .....	vi
List of Figures .....	viii
Abstract.....	ix
Chapter 1: Introduction .....	1
1.1: Why Biofuels? .....	1
1.2: Biomass Thermal Degradation Processes.....	2
1.3: Product Upgrading Pathways .....	4
1.4: Separation of Torrefaction Products .....	5
1.5: Characteristics of Activated Carbon .....	6
Chapter 2: Adsorption Bed Chromatography Experiments.....	20
2.1: Experimental Apparatus .....	20
2.2: Theoretical Background of Adsorption.....	23
2.3: Experimental Procedure and Chromatogram Analysis.....	23
2.4: Experiment Design, Results, and Discussion .....	26
Chapter 3: Adsorptive Capacity and Capacity Loss Experiments .....	42
3.1: Experimental Apparatus .....	42
3.2: Experimental Procedure and Data Analysis.....	43
3.3: Experiment Design, Results, and Discussion .....	46
3.4: Industrial-Scale Temperature-Swing Adsorption Process Design .....	57
Chapter 4: Conclusions and Future Work.....	64

4.1: Conclusions of Chromatography, Capacity, and Capacity Loss Experiments	
.....	64
4.2: Future Work.....	65
References .....	68

## List of Tables

Table 1. Retention time data at various temperatures .....	21
Table 2. Fitted kinetic parameters using retention time data .....	22
Table 3. Capacity estimates used to fit kinetic parameters.....	22
Table 4. Representative compounds and their structures, functionalities, and concentrations .....	28
Table 5. Control data and chromatographic experimental data .....	31
Table 6. Chromatography data for acetic acid and <i>m</i> -cresol binary mixture .....	36
Table 7. Chromatography data for acetic acid and benzene binary mixture .....	37
Table 8. Short column chromatography data .....	40
Table 9. Carbon sample numbers and descriptions .....	46
Table 10. TGA/DSC data for IPA on several carbon samples .....	47
Table 11. TGA adsorption data for several representative compounds .....	52
Table 12. Process condition upper and lower bounds .....	59
Table 13. Process parameters for various cases.....	60
Table 14. Cases with torrefaction parameters advantageous for separations .....	62
Table 15. Bed proportions for cases G and H .....	63

## List of Figures

Figure 1. Temperature ranges of cell wall biopolymer thermal fractionation .....	3
Figure 2. Product distribution of stage 1 (torrefaction) product.....	4
Figure 3. Sketch of graphitic morphology (left) and amorphous morphology (right) .....	8
Figure 4. A selection of oxygenated surface functionalities.....	9
Figure 5. GC oven and example of column .....	11
Figure 6. GC plug travel cartoon .....	18
Figure 7. A typical PeakSimple chromatogram .....	25
Figure 8. Change in <i>m</i> -cresol peak area with number of runs.....	41
Figure 9. Typical TGA plot .....	45
Figure 10. Adsorption enthalpy for carbon samples via TGA/DSC .....	48
Figure 11. Adsorption enthalpy for carbon samples via TGA/DSC .....	54
Figure 12. Change in acetic acid peak area with number of runs .....	54
Figure 13. Change in <i>m</i> -cresol retention time with number of runs.....	55
Figure 14. Change in <i>m</i> -cresol peak area with number of runs .....	55
Figure 15. Adsorptive separation process diagram .....	63



## Abstract

Biofuels processes involve the upgrading of components produced by fractionation of cell wall biopolymers. However, the fractionation is not selective to high-value components, and separation is necessary. The use of adsorptive separations for biofuels mixtures avoids oligomerization reactions caused by thermal separations. Activated carbon strongly adsorbs phenol derivatives but weakly adsorbs acetic acid, which makes it a strong candidate for biofuels separations. This work investigated the adsorption characteristics of several representative compounds onto activated carbon, and probed the suitability of activated carbon for biofuels separations processes. An activated carbon packed bed was used for chromatography studies, and a modified TGA/DSC was used to study adsorption capacity and thermodynamics. It was found that phenolic compounds such as *m*-cresol likely adsorb via a combined hydrogen bonding and  $\pi$ - $\pi$  stacking mechanism to surface sites such as quinones, as well as less strongly to flat carbon ring sites via  $\pi$ - $\pi$  stacking alone and to oxygenated sites via hydrogen bonding alone. In contrast, aromatic compounds such as benzene adsorb via  $\pi$ - $\pi$  stacking only, and light oxygenates such as acetic acid adsorb via hydrogen bonding only. The adsorptive capacity found for *m*-cresol, the representative phenolic target for adsorptive separations, was between 12.0 and 24.6 g/kg adsorbent, or between 0.111 and 0.227 mol/kg adsorbent. This work also finds a characteristic breakthrough curve for *m*-cresol on activated carbon, and designs a scaled-up adsorptive separation process including adsorbent regeneration.

## Chapter 1: Introduction

### *Why Biofuels?*

For over 100 years, gasoline-powered vehicles have been a major mode of transporting people and goods. That gasoline overwhelmingly originates as oil, which is extracted from limited reserves, then refined into gasoline and other products. Public estimates on the amount of oil which can still be extracted range from roughly 50 years [1], using only proven reserves, to more than 100 years, speculating that other reserves will be found or exploited during that time.

More concerningly, research has repeatedly shown that petroleum-derived fuels are the largest contributing factor to the recent increase in atmospheric CO<sub>2</sub>, which is the largest source contributing to anthropogenic global climate change [2-5]. Global climate change is already leading to a loss of global biodiversity, adverse effects on food crops, and even loss of human life [6-11]. Therefore, a solution to the problem of limited transport fuels must also solve the problem of increasing atmospheric CO<sub>2</sub>.

However, a further constraint must apply. Especially in America, transport infrastructure is largely designed around liquid fuels. Liquid fuels confer several advantages over other forms of energy suitable for transport use: they are extremely energy-dense, they are simple to transfer from a central source to a vehicle, and they can be stored at atmospheric conditions for a long time without appreciably degrading [12, 13].

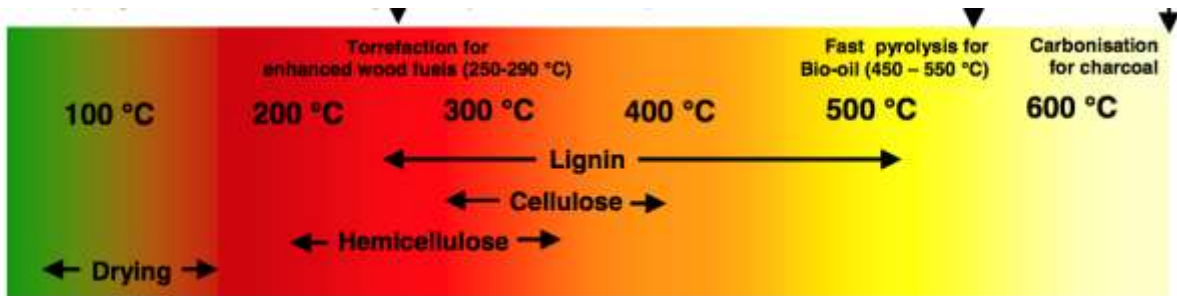
With these requirements in mind, biofuels present a viable solution to the problem of limited transport fuels. Biofuels processes can produce enough quantity of transport fuels to

satisfy a significant proportion of demand, biofuels processes can be designed which are carbon-neutral, and the results of those processes can be liquid fuels, similar in chemical makeup to the fuels in use already. Furthermore, biomass-based processes have shown promise for replacing other products which are currently petroleum-based, such as plastics, lubricants, and other petrochemicals.

### *Biomass Thermal Degradation Processes*

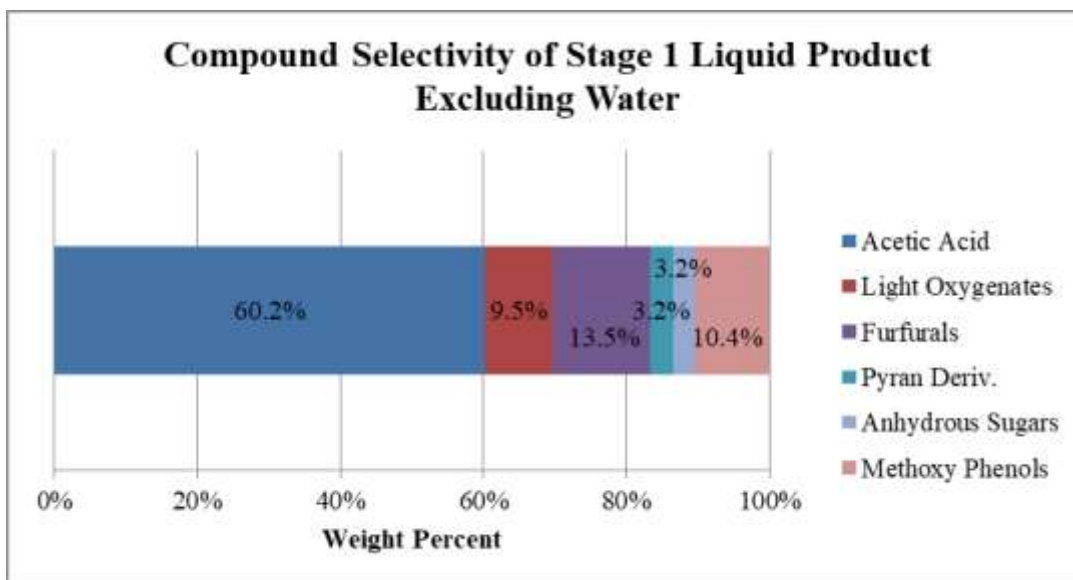
Plant-derived biomass is primarily composed of three groups of polymeric components: cellulose, hemicellulose, and lignin [14]. Cellulose is made up of anhydrosugar monomers, and decomposes at moderate temperatures (300-400°C), as shown in Figure 1 on the next page [15]. Hemicellulose is made up of a variety of light oxygenate monomers, including furans, pyrans, furfurals, and carboxylic acids. Hemicellulose decomposes at low temperatures (200-350°C) [15]. Lignin is found in three main types, each of which is composed of a different kind of phenolic monomer. *S*-type lignin is made up of syringyl monomers, *G*-type lignin is made up of guaiacyl monomers, and *H*-type lignin is made up of *p*-hydroxyphenyl monomers [14]. Lignin decomposes at similar temperatures to hemicellulose, which means that when whole biomass is thermally decomposed, a variety of chemical categories are produced simultaneously [15]. Lignin, unlike cellulose, is characterized by a variety of linkages between monomer units, giving rise to a non-uniform structure [14, 15]. Cross-linkages between lignin units also contribute to its macroscopic properties, and cross-linkages between lignin units and cellulose and

hemicellulose units make the decomposition of plant-derived biomass a complicated subject of study [14, 15].



**Figure 1: Temperature ranges of cell wall biopolymer thermal fractionation**

There are two major categories of biomass thermal degradation processes: torrefaction and pyrolysis. Torrefaction generally occurs at low temperatures (250-290°C), and is characterized by decomposition of primarily hemicellulose. Pyrolysis occurs at higher temperatures, and is characterized by more complete decomposition of all polymeric components of plant-derived biomass. The product composition of bench-scale torrefaction of red oak is shown in Figure 2 on the following page [16].



**Figure 2: Product distribution of Stage 1 (torrefaction) liquid product**

Since the different biopolymers in plant-derived biomass tend to decompose at different temperatures and into products of different functionality, several strategies to improve the selectivity of thermal fractionation of plant-derived biomass have been suggested. The most promising such strategy is to carry out the thermal fractionation in stages, which will tend to segregate products based on the specific biopolymer from which they originate [15]. However, even staged thermal fractionation cannot segregate products originating from biopolymers which decompose at similar temperatures, such as anhydrosugars from hemicellulose and phenolics from lignin.

### *Product Upgrading Pathways*

The leading proposed strategies for upgrading torrefaction products tend to involve a ketonization step and an aldol condensation step for the carboxylic acids derived from

hemicellulose [17, 18]. These reactions are proposed to be carried out on expensive metal oxide or oxide-supported metal catalysts, such as titania or ruthenium supported on titania [18]. If these reactions are carried out using a mixture of stage 1 torrefaction products, then the phenolic content of the mixture tends to cause coking. Furans and anhydrosugars, which are also cellulose and hemicellulose derivatives, can also undergo deoxygenation reactions to form coke [19, 20]. Coke formation deactivates the catalyst by blocking access to active sites, and so it is desirable to use a reaction mixture which is not prone to coking.

In addition, phenolic products derived from lignin can be hydrogenated and undergo ring opening to form fuel-range alkanes and cycloalkanes [21]. The potential for upgrading phenolics and the potential to avoid coking present a compelling reason to develop separations strategies for stage 1 torrefaction mixtures.

### *Separation of Torrefaction Products*

The simplest generally applicable separation strategy is typically thermal separation. Either by flash evaporation or staged distillation, thermal separation exploits boiling point differences to separate a mixture by selectively changing its phase. However, thermal separation is not viable for torrefaction products because heating the mixture increases the rate of an undesirable oligomerization reaction [18].

When thermal separation is infeasible, a frequent alternative is to manipulate pressure in order to accomplish separation by the same means. At low enough pressures, two liquids may phase-separate, and at high enough pressures, two gases may phase-separate. But stage 1

torrefaction mixtures contain several classes of components. Within each class, different components have different boiling points, and the boiling points of components in different classes overlap. Since the aim of a separations strategy for torrefaction mixtures is to separate components by class for targeted upgrading, and there are dozens of individual components in such a mixture, pressure-based separations must either be non-selective or unreasonably expensive, and therefore undesirable.

Another alternative to phase-based separation is adsorption. Adsorptive separation exploits differences in interaction with an adsorbent between multiple components or classes of component to separate those components. Since the aim of a separations strategy for torrefaction mixtures is to separate components by class for targeted upgrading, separation by adsorption, and therefore by component class, is likely to work.

Since phenolic products can be upgraded separately from the other stage 1 torrefaction products, are not the major product of stage 1 torrefaction, and also interfere with the upgrading of other stage 1 torrefaction products, targeting the choice of adsorbent at adsorbing phenolics is reasonable. In addition, to accomplish effective separation, the adsorbent material should be relatively cheap, and should have a high adsorption capacity on a weight basis. Activated carbon meets all these criteria for a good choice of adsorbent.

### *Characteristics of Activated Carbon*

Activated carbon is produced by chemical activation of carbonaceous material. Many feedstocks can be used, such as amorphous coal, charred wood (often called activated

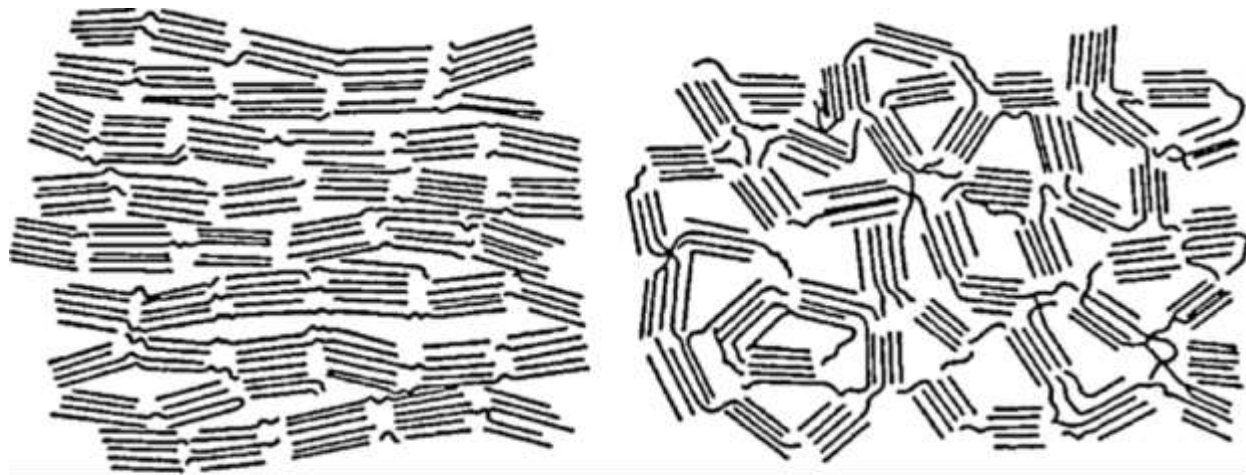
charcoal), and even nutshells [22]. There are two main steps in producing activated carbon: carbonization and activation. The carbonization step removes impurities from the carbon, such as heteroatoms and hydrogen, and is carried out at relatively high temperatures, around 800°C, and in an oxygen-poor environment [23]. The removal of these impurities creates a pore structure within the material. The activation step involves an oxidizing atmosphere, such as air, CO<sub>2</sub>, or steam, and very high temperatures (950-1000°C). Activating the carbonized material alters the pore structure by opening pathways to internal pore spaces, and creates oxygenated surface groups, which can interact with potential adsorbates [23]. Since staged thermal fractionation is carried out on carbonaceous material, and stage 3 pyrolysis leaves behind char, it could be feasible to integrate the production of the activated carbon adsorbent into the biofuels process, reducing waste and costs.

The internal pore space unlocked by activation results in a typical surface area of 800-1500 m<sup>2</sup>/g. Around 95% of the surface area is microporous surface area, contained in pores with radius smaller than 2 nm. Another 5% is mesoporous surface area, contained in pores with radius smaller than 50 nm, and the remainder is macroporous surface area, contained in pores with radius larger than 50 nm. Macroporous surface area is nearly zero, which indicates that macropores are mostly channels through which adsorbates travel to reach meso- and microporous sites [23].

The chemical and adsorptive characteristics of an activated carbon surface do not depend strongly on its morphology, but the main categories of activated carbon morphology merit discussion nonetheless. The most common category is amorphous carbon, characterized by random, non-ordered structure. Also relatively common is graphitic carbon, characterized by



sheet-like, regular formations. Figure 3 below illustrates the structural differences between graphitic and amorphous activated carbon morphologies [23, 24].



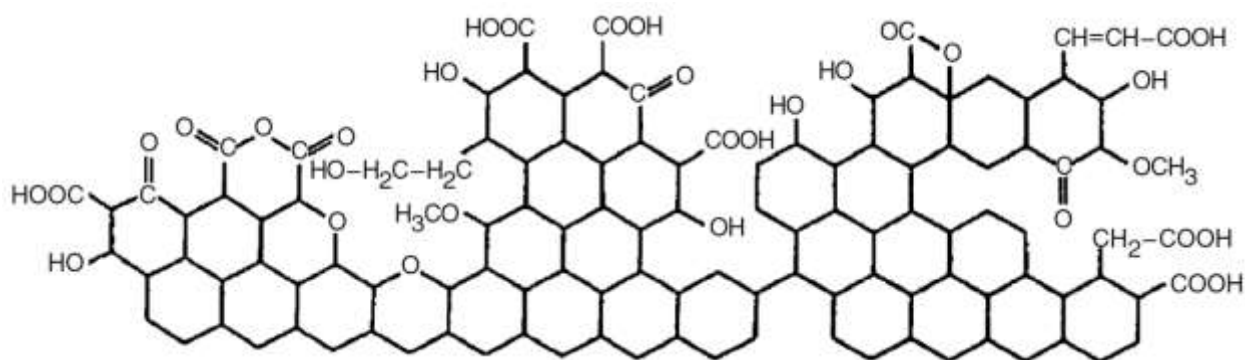
**Figure 3: Sketch of graphitic morphology (left) and amorphous morphology (right)**

Since the pore structure of an activated carbon is developed during the activation process, it does not strongly depend on the morphology of the carbon used. Instead, the heteroatom content of the original carbonaceous material dictates the microporosity, with larger amounts of heteroatoms leading to a larger concentration of micropores; and the length of activation determines the meso- and macro-porosity, as well as the accessibility of the microporous surface area, by oxidizing away the carbon walls separating pore spaces [23].

During the activation step, the oxidizer burns away carbon in the pore structure, leading to widening of pore mouths and channels, interconnection between pores, and better access to the microporous structure that contains the majority of active surface area. But besides improving access to surface sites, the oxidizer is also responsible for creating surface sites. Before activation, the carbon surface is mostly devoid of oxygen-containing groups. The

activation step oxidizes some surface carbon which is not burned off completely. The result is oxygen-containing surface groups which can act as active sites to adsorb some materials [23].

The chemical identity of these oxygen-containing surface groups varies. Some form carbonyl groups, others incorporate a carbon ring structure and form chromene or pyrone groups, and others form carboxylic acid, ether, or ester groups. Examples of many possible oxygenated surface structures for activated carbon are illustrated in Figure 4 below [23].



**Figure 4: A selection of oxygenated surface functionalities**

Thermal desorption studies have been performed on activated carbons, with disagreeing results. One set of authors argues that low temperatures (200-600°C) decompose phenols and carboxyls and form water vapor, moderate temperatures (350-750°C) decompose carboxyls and lactones into CO<sub>2</sub>, and high temperatures (500-1000°C) decompose quinones and phenols into CO, as well as out-gassing hydrogen by splitting C-H bonds directly [23]. However, other authors argue that even at low temperatures, surface carboxylic groups rearrange into other surface groups, in addition to partial decomposition into water vapor [23, 25].

This work focuses on the adsorptive characteristics of porous activated carbon, and its application for biomass thermal degradation product separations.

## Chapter 2: Adsorption Bed Chromatography Experiments

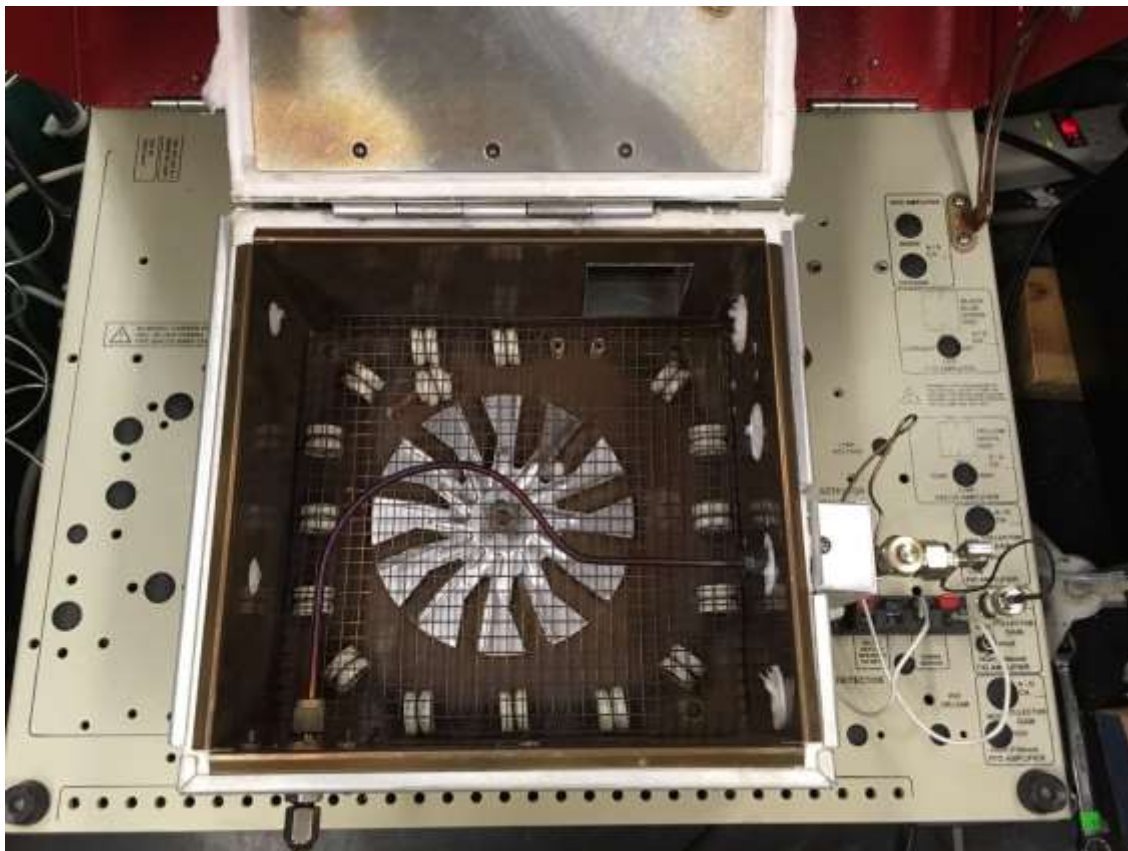
### Experimental Apparatus

#### *GC Adsorbent Bed Apparatus*

A gas chromatograph (SRI model 8610C) equipped with an in-line flame ionization detector (FID; SRI for model 8610C GC) was used to study the adsorption of several compounds on activated carbon (Sigma-Aldrich 20-40 mesh). A 1/8-inch OD, 3/32-inch ID stainless steel tube 12 inches in length was packed with the adsorbent material, gently vibrated to settle the adsorbent particles, and then gently compacted with a ramrod to diminish bed void fraction. The ends of the tube were plugged with small amounts of fibrous glass wool to prevent any activated carbon from falling out of the tube during installation or operation. Because of the glass wool plugs capping the tube ends, the full 12 inches of tubing were not available for use. In addition, to accommodate a variety of separation strategies, some columns were not completely filled with adsorbent material. In the cases of these columns, the glass wool plug at the column entry was pushed along the tube until it contacted the activated carbon. This ensured that the bed did not shift further downstream during operation due to a constant flow of gases. For various experiments, new adsorption beds were packed, and the characteristics of the bed used for each experiment are indicated appropriately in the methods section, including weight of activated carbon adsorbent, column length filled with adsorbent, and the bulk density of adsorbent and bed void fraction that resulted from the length and weight of packed adsorbent. In order for the column containing the adsorption bed to fit inside the GC oven, the column was bent gently into a U-shape followed by an L-shape, so that the inlet and outlet

could be attached to the injection port and the FID unit, respectively, using Swagelok fittings.

Figure 5 below shows the GC oven with column fitted.



**Figure 5: GC oven and example of column**

The carrier gas used for all chromatography studies was nitrogen (Airgas Ultra-High Purity Nitrogen) at 25 psig, controlled by the GC's internal flow controller to 150 mL/min. The FID was operated using 250 mL/min of air (Airgas Zero Air) and 25 mL/min of hydrogen (Airgas Ultra-High Purity Hydrogen). Swagelok 1/8-inch stainless steel tubing conveyed all gases from their respective pressure regulators to the GC inlets as appropriate. The same pressure regulators were used for every experiment to supply each gas, and were never removed from the tubing leading to the GC or altered in any way. The same FID was used for every

experiment, and it was never removed or altered. The air and hydrogen flows supplying the FID were not subject to any changes when the column was changed, because the flow paths of the air and hydrogen did not involve the column. However, the nitrogen carrier gas did flow through the column, and because it was impossible to ensure that each column was packed identically, slight adjustments were made to the GC's flow controller so that a constant 150 mL/min flow rate could be achieved. Occasionally, the flow pattern arising from the packing of a particular column would lead to the carrier gas blowing out the FID flame. In these instances, the column was rejected during calibration (before any experiments were performed) and replaced with a similar column that did not extinguish the FID flame.

Calibration was performed for each gas separately. Flow rate of each gas was measured by the rate at which a thin film of surfactant traveled along a wetted column of known volume, propelled solely by the gas being measured (bubble flowmeter). Since all gases shared a common, single exit point at the FID outlet, the bubble flowmeter was connected via a flexible tube to the FID outlet. While checking each gas flow rate, the other gases were shut off at the cylinder. In order to limit changes to as few variables as possible, the pressure at the regulator was not adjusted unless the regulator pressure gauge read a different value than the 25 psig supply required by the GC. Because the regulator pressure was not adjusted, it was necessary to allow excess pressure to bleed off before calibrating the flow rate of a different gas. It was found that for the air and hydrogen supplying the FID, flow rate was very consistent, with an observed variance of less than 2% over several measurements. However, the nitrogen carrier gas, which flowed through the adsorbent bed prior to measurement, was subject to a larger variance in flow rate which approached 5%.

Sample injections were performed using a Hamilton 10  $\mu\text{L}$  glass syringe through the built-in injection port on the front of the GC. A septum was used to seal the aperture and ensure that the only path the sample could take was through the adsorption column and the in-line FID. Since all samples were drawn from their sources at room temperature and pressure, most samples were liquid, although a few exceptions were gas. Since the samples were drawn at room temperature and the GC oven was usually held at a higher temperature, the samples expanded in the injection port as they were rapidly heated to the GC's steady-state temperature. For liquid samples, this included the volume change of vaporization. Very rarely, the volume change of a vaporizing sample increased the inlet pressure enough to blow out the FID flame. For this reason, the largest liquid sample size used was 5  $\mu\text{L}$ .

### **Theoretical Background of Adsorption Chromatography**

Two kinds of adsorption are common: physical adsorption and chemical adsorption. Physical adsorption (physisorption) is similar to a phase change process, wherein the van der Waals interactions between one component in a fluid phase and the adsorbent overcome the van der Waals interactions between that component and the other components in the fluid phase. Physisorption is a purely thermodynamic process, and does not involve an activation barrier. Physisorption is commonly observed on activated carbons.

Since physisorption is a purely thermodynamic process, it is controlled by thermodynamic variables. The primary equation governing any thermodynamic process is the

relation between enthalpy change, entropy change, temperature and Gibbs free energy change, given in Equation 1 below.

$$\Delta G_{ads} = \Delta H_{ads} - T\Delta S_{ads} \quad \text{Equation 1}$$

For any adsorption process, the entropy change is always negative. The fluid phase must be more disordered than the adsorbed phase, because adsorption involves the loss of degrees of freedom. Temperature must always be positive, so the  $-T\Delta S$  term must always be positive. At temperatures at which adsorption occurs spontaneously, the Gibbs free energy change must be negative, which means that spontaneous adsorption is always exothermic.

Chemical adsorption (chemisorption) is similar to a chemical reaction, wherein fluid-phase components interact chemically with the adsorbent surface. Because chemisorption is a chemical process, it does involve an activation energy. Chemisorption is often reversible, which means equilibrium kinetics are appropriate mathematical descriptions of chemisorption. However, because surface sites act as “reactants” in chemisorption processes, a separate surface kinetic model which accounts for the limited number of available surface sites must be used. The Langmuir adsorption model is sufficient to describe the chemisorption processes involved in these experiments. The basic form of the Langmuir adsorption model is given in Equation 2 below.

$$\theta_A = \frac{K_A P_A}{1 + K_A P_A} \quad \text{Equation 2}$$

In the Langmuir chemisorption model,  $\theta$  represents the equilibrium coverage of an adsorbate on the surface, expressed as a fraction of the total available sites occupied by that adsorbate.  $P$  represents the partial pressure of an adsorbate in the gas phase.  $K$  represents the

adsorption equilibrium coefficient, which varies exponentially with temperature according to the van 't Hoff equation for equilibrium processes, given as Equation 3 below. It follows trivially from the Langmuir expression that the equilibrium coverage at a very high partial pressure of adsorbate approaches 1, meaning that nearly all surface sites to which the adsorbate can adsorb are occupied.

$$K = K_0 * \exp \left[ \frac{-\Delta H_{ads}}{R} \left( \frac{1}{T} - \frac{1}{T_0} \right) \right] \quad \text{Equation 3}$$

In the van 't Hoff equation, the adsorption equilibrium coefficient  $K$  is expressed as a function of temperature, using a known reference adsorption equilibrium coefficient  $K_0$  for a reference temperature  $T_0$ . The van 't Hoff equation assumes that the adsorption process is truly reversible; that is, that the enthalpy of the transition state is exactly the same for both the forward process and the reverse process. This assumption leads to the result that neither the activation energy for adsorption nor the activation energy for desorption need be known, only the enthalpy change due to adsorption. The van 't Hoff equation also assumes that the enthalpy change due to adsorption is not itself a function of temperature. Because the enthalpy change for any spontaneous adsorption process is always negative, it follows from the van 't Hoff equation that the adsorption equilibrium coefficient  $K$  must be lower at higher temperatures. Therefore, for a constant partial pressure of adsorbate, the equilibrium coverage must decrease as temperature increases.

Experimentally, the adsorption equilibrium coefficient  $K$  can be obtained for a constant temperature by manipulating the partial pressure of the adsorbate. At very low partial pressures, the product  $K_A P_A$  is much smaller than 1, so a change in partial pressure produces a



linear change in coverage whose slope depends on K. Once the adsorption equilibrium coefficient has been found at several temperatures, the enthalpy change due to adsorption can be found by linear regression. Assuming the enthalpy change due to adsorption does not vary with temperature, once it has been found, the adsorption equilibrium coefficient can be obtained for any temperature. Technical challenges involved with measuring coverage, and thereby the adsorption equilibrium coefficient, are discussed in depth in Chapter 3.

However, for these experiments, the equilibrium coefficient is not the most important quantity. The measured peak areas included very long tails, representing the desorption of almost all of each component. The equilibrium adsorbed amount in these cases approached zero, because the partial pressure in the gas phase as desorption went on approached zero. While the material was carried down the column, the rate of adsorption tended to be much faster than the rate of desorption. This is why the retention time was longer for each compound on an activated carbon column than on a glass wool column, as described below. A theoretical mathematical model was developed which described the phenomena involved in these experiments, and which could be used to find the enthalpy change due to adsorption for a non-equilibrium process.

First, for a single adsorbate A, the mass adsorbed onto the entire column per gram of adsorbent  $q_A$  varies with time, in a manner described by equation 4 below:

$$\frac{dq_A}{dt} = r_a - r_d = k_a P_A \theta_v - k_d \theta_A \quad \text{Equation 4}$$

Where the subscript  $a$  denotes adsorption, and the subscript  $d$  denotes desorption. Equation 4's right hand side uses the Langmuir model to describe the rates of adsorption and desorption

in terms of the coverage of A. Because only one adsorbate is involved,  $\theta_v = 1 - \theta_A$ . If the maximum potential amount of A adsorbed is called  $q_m$ , and represents the amount adsorbed if all adsorption sites available for A on the entire column are occupied by A, then the following expression for  $\theta_A$  is valid:

$$\theta_A = \frac{q_A}{q_m} \quad \text{Equation 5}$$

This expression can be substituted into equation 4 along with the expression for  $\theta_v$  to yield a differential equation describing the relationship between amount adsorbed and time using only those two quantities, constants, and experimentally variable parameters:

$$\frac{dq_A}{dt} = k_a P_A \left(1 - \frac{q_A}{q_m}\right) - k_d \frac{q_A}{q_m} \quad \text{Equation 6}$$

It should be noted that the kinetic rate constants  $k_a$  and  $k_d$  are not constant, but vary with temperature according to the activation energy for the adsorption and desorption processes. For the purposes of this model's development, the Arrhenius equation for the variance of kinetic rate constants with temperature was assumed to be valid. It was assumed for all adsorbates that the adsorption rate constant was much larger than the desorption rate constant, and thus that the rate-limiting step of the adsorbate's progress down the column was desorption. Mathematically, this is expressed as  $k_a \gg k_d$ . It follows that as long as the total amount of adsorbate injected onto the column does not exceed the total capacity for adsorption of that adsorbate, then the partial pressure will be nearly zero and the change in amount adsorbed with respect to time will be nearly zero.

For the development of this model, it was assumed that the adsorbed A furthest upstream was desorbed first, and that the carrier gas flowrate was so large, and the adsorption rate constant so much larger than the desorption rate constant, that desorbed A traveled to the first available adsorption site further downstream and immediately adsorbed. This assumption simplifies the mathematics, reducing a system of higher-order partial differential equations into a single, separable, ordinary differential equation. A cartoon illustrating this assumption is presented in Figure 6 below. The dark red segment indicates adsorbed material, the horizontal arrow indicates the direction of carrier gas flow, the thin light red segment indicates material about to desorb, and the thin green segment indicates where the desorbed material will re-adsorb almost instantaneously.



**Figure 6: GC plug travel cartoon**

With these assumptions, it can be seen that the sites available for adsorption within the “plug” of adsorbate as it travels down the column are completely occupied by adsorbate, while all other sites are completely empty. The rate of travel down the column is constant, and depends on the rate of desorption, regardless of the rate of adsorption. The amount adsorbed on the column is constant from the moment the last molecule of injected adsorbate enters the column to the moment the first molecule leaves the column. Less obviously, the rate of desorption is constant during that same period. Because the rate of desorption depends on the

amount adsorbed, and the amount adsorbed is constant during that period, the rate of desorption must be constant. To describe the rate of desorption after the plug of adsorbate reaches the end of the column, further theoretical development is required.

When the front of the plug of adsorbate reaches the end of the column, the rate of adsorption must be zero according to the assumptions listed above. No sites are available downstream from desorbed material, so the only possible destination for that material is out the end of the column, to be recorded on the FID. Therefore, the rate of change of amount adsorbed is equal to the rate of desorption only:

$$\frac{dq_A}{dt} = -k_d \frac{q_A}{q_m} \quad \text{Equation 7}$$

This equation can be integrated to obtain an expression for  $q_A$  as a function of time:

$$q_A(t) = C \exp\left[\frac{-k_d t}{q_m}\right] \quad \text{Equation 8}$$

Where C is an integration constant that can be evaluated using a boundary condition. Since the amount adsorbed must be exactly equal to the amount injected for all times between injection and the time when the front of the plug reaches the end of the column, set the time when the front of the plug reaches the end of the column as  $t = 0$ . The mass adsorbed at time  $t = 0$  must be equal to the amount injected:

$$q_A(0) = \frac{V_A \rho_A}{w_{ads}} = C \exp(0) = C \quad \text{Equation 9}$$

Where V is the injection volume and  $w_{ads}$  is the total mass of adsorbent in the column. The only unknown parameters in the resulting expression are  $k_d$  and  $q_m$ , which can be found by

experimentation. The capacity measurements presented in Chapter 3 attempt to resolve the value of  $q_m$  for various adsorbates under various conditions, and some analysis of data collected by Schneberger was conducted to estimate how  $k_d$  varies with temperature [26].

In order to analyze old data, the mathematical model must be further developed to determine how the desorption rate changes with temperature and how that influences the retention times. It follows from the assumptions regarding desorption and re-adsorption that every site must be occupied exactly once. Therefore, the time required for the plug to travel the length of the column depends on the number of times each molecule must adsorb individually – or, in different terms, the number of times one plug can fit into the column. Note that because adsorption is assumed to be nearly instantaneous, at the instant of injection, the adsorbate already occupies one full “plug-length” of adsorbent. In addition, at the instant the front of the plug reaches the end of the column, the maximal rate of desorption occurs. Because the FID chromatogram shows the amount leaving the column as a function of time, and the retention time is recorded as the time at which the largest amount leaves the column, these assumptions lead to the conclusion that the retention time is the instant the front of the plug reaches the end of the column. Therefore, the recorded retention time can be compared to the injection mass and the measured capacity for the adsorbate in order to fit kinetic rate parameters to the expression for desorption:

$$retention\ time = \frac{\left[\frac{q_m-1}{q_A}\right]}{\left[\frac{k_d q_A}{q_m q_A}\right]} = \frac{\left[\frac{q_m-1}{q_A}\right]}{\left[\frac{k_d}{q_m}\right]} = \frac{q_m \left[\frac{q_m-1}{q_A} - 1\right]}{k_d} = \frac{q_m \left[\frac{q_m-1}{q_A}\right]}{k_d^0 \exp\left[\frac{-E_d}{R}\left(\frac{1}{T} - \frac{1}{T^0}\right)\right]} \quad \text{Equation 10}$$

Where  $E_d$  is the activation energy for desorption,  $k_d^0$  is the rate constant at temperature  $T^0$ , and those two parameters can be fitted to data taken at multiple temperatures, with all else held constant.

The data used to fit those two parameters are given in Table 1 below [26].

Compound	Retention Time at 250 °C (s)	Retention Time at 300 °C	Retention Time at 350 °C	Retention Time at 380 °C
Syringol			216	102
Levoglucosan		522	150	
Guaiacol	303	75		
m-Cresol	297	54		
Furfural	174	111		
Acetic Acid	51	12		
Pyran	36	15		

**Table 1: Retention time data at various temperatures**

Similarly, the fitted parameters for each component under different cases are given in Table 2 on the following page. The capacity estimates used for each component were found in the work presented in chapter 3 or in the literature. The low estimate was found using the TG experiments described in chapter 3. The high estimates are based on the highest capacity found in the literature for any of these components on activated carbon, and the components found to have a lower capacity with TG experiments had their estimates reduced accordingly. The medium estimates are approximately interpolated logarithmically from the high and low estimates. The capacity estimates are given in Table 3 on the following page.

Compound	Desorption Energy (kJ/mol)	Scale Factor at T <sup>0</sup> , low capacity estimate (g*s/g)	Scale Factor at T <sup>0</sup> , medium capacity estimate	Scale Factor at T <sup>0</sup> , high capacity estimate
Syringol	84.63	4.34 E-5	1.12 E-3	0.0782
Levoglucosan	74.06	7.69 E-6	2.85 E-4	0.0209
Guaiacol	69.61	3.05 E-5	7.91 E-4	0.0552
m-Cresol	62.97	3.76 E-5	8.76 E-4	0.0608
Furfural	22.41	-3.42 E-6	1.75 E-4	0.0227
Acetic Acid	72.14	-4.05 E-6	6.20 E-5	0.0210
Pyran	43.65	-6.12 E-6	9.95 E-5	0.0315

**Table 2: Fitted kinetic parameters using retention time data**

Compound	Low estimate (g/g)	Medium estimate	High estimate
Syringol	0.006	0.025	0.2
Levoglucosan	0.006	0.025	0.2
Guaiacol	0.006	0.025	0.2
m-Cresol	0.00616	0.025	0.2
Furfural	0.001	0.01	0.1
Acetic Acid	0.00023	0.004	0.05
Pyran	0.00025	0.004	0.05

**Table 3: Capacity estimates used to fit kinetic parameters**

Since it has been assumed that the rate constant for desorption is much smaller than the rate constant for adsorption, it follows from the Arrhenius equation for variance of the rate constant with temperature that, independent of temperature, the activation energy for adsorption is much smaller than the activation energy for desorption. Because the enthalpy change due to adsorption is equal to the difference between the activation energy for desorption and the activation energy for adsorption, this method of analysis should not be considered to yield the true enthalpy of adsorption.

## Experimental Procedure and Chromatogram Analysis

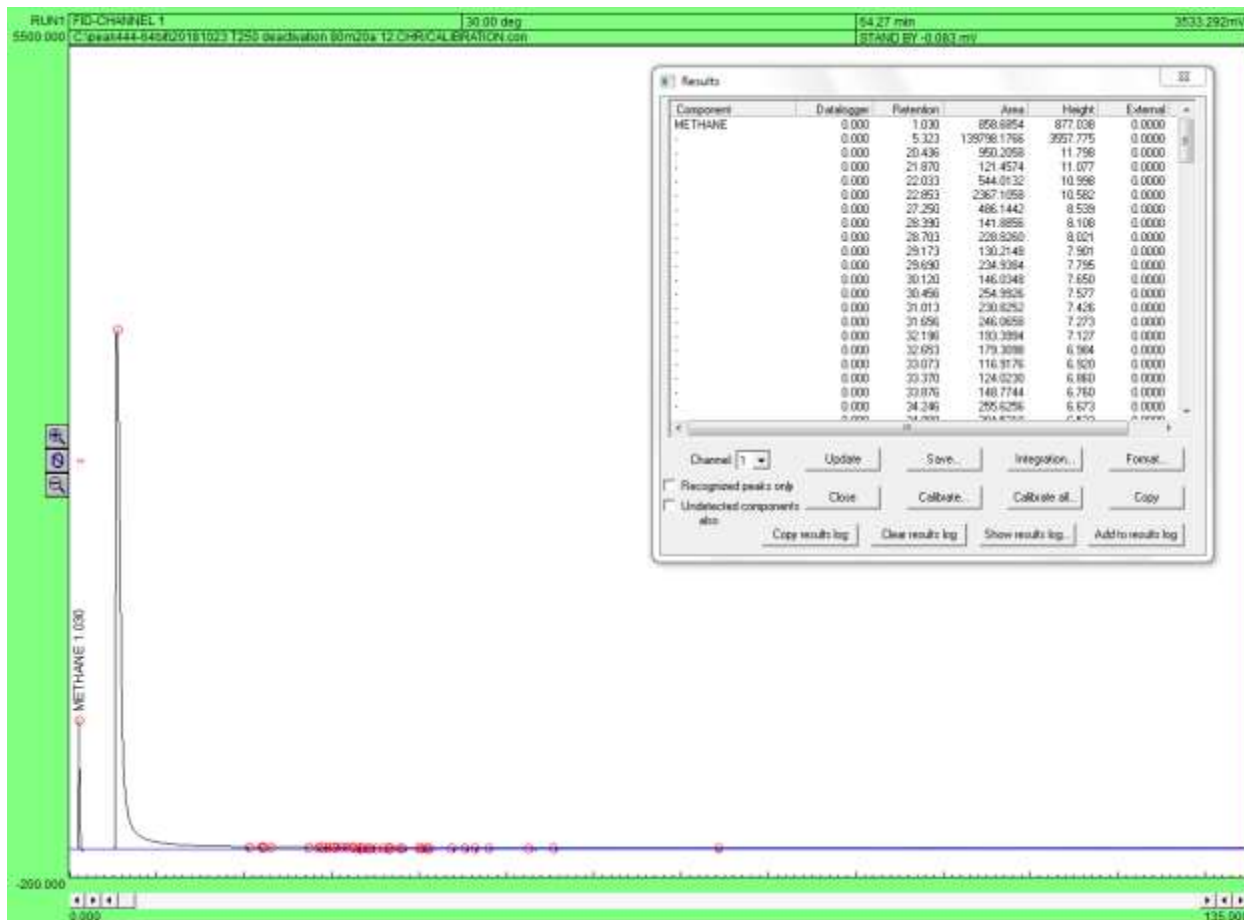
At  $t = 1.00$  min of each run,  $5 \mu\text{L}$  of methane was injected onto the column to confirm that the FID was functioning properly. Methane was selected because it was readily available, cleared the column completely within a few seconds, and formed a sharp, narrow, symmetric, repeatable peak with almost no tail, indicating that it did not interact with the activated carbon. At  $t = 5.00$  min of each run, the sample was injected onto the column. Retention times reported in the data and analysis sections of this document have been corrected to account for the time of injection.

FID data was collected and analyzed using PeakSimple version 4.44 for a 32-bit Windows 7 operating system. The PeakSimple program automatically identified peaks and reported the total area and retention time for each. The peak area is defined as the integral of the function which generates the peak, taken from the time at which the peak begins to the time at which it ends. Given that no simple explicit function can be constructed which generates any particular peak, the PeakSimple program approximates the function using a numerical integration method. The units of retention time are reported here in minutes, and the units of peak area are reported here in mV-cmin (millivolt-centiminutes), an arbitrary unit based on the signal recorded by the FID. Peak area may be reported without a unit labelled, because FID response varies slightly for each analyte, and can be compared directly to standard amounts of each analyte to calculate the amount of analyte present.

An example of a typical PeakSimple chromatogram is shown in Figure 6 on the following page. This chromatogram is of a  $5\mu\text{L}$  sample which is 80% acetic acid and 20% *m*-cresol by



volume, for a total of 4  $\mu\text{L}$  of acetic acid and 1  $\mu\text{L}$  of *m*-cresol in the mixture. It was injected at  $t = 5.00$  min, at a column oven temperature of 250  $^{\circ}\text{C}$ . A methane standard was also injected at  $t = 1.00$  min, as per the standard procedure. The earlier peak is methane, and the later peak is acetic acid. The *m*-cresol is not visible here, as it did not elute until a 350  $^{\circ}\text{C}$  bakeout was performed for this run. Assignment of peak area to the correct components was challenging, but a consistent method was devised to analyze all chromatograms. The PeakSimple integration settings were adjusted to minimize the number of false positive peaks (the red circles which appear along the baseline of Figure 6). If PeakSimple's peak identification was too aggressive, many false positive peaks were identified. If identification was not aggressive enough, PeakSimple would fail to identify wide, flat peaks. Once the integration settings produced satisfactory results for a variety of real peak configurations, those settings were applied to all chromatograms. However, those settings could not eliminate false positive peaks.



**Figure 7: A typical PeakSimple chromatogram**

Because the integration tool was set to keep the baseline at zero, and the integration tool does not assign any area to multiple identified peaks, the area of each identified peak could be uniquely assigned to a particular analyte. Each identified peak was assumed to belong to a single analyte. The retention time of an analyte was recorded as the time of the highest identified peak assigned to that analyte. The boundary between analytes was drawn at the time of the lowest identified peak between the two highest identified peaks assigned to those analytes. All peaks later than the retention time of the earlier analyte and earlier than the boundary, including the boundary peak, were assigned to the earlier analyte. All peaks later than the boundary peak and earlier than the retention time of the later analyte were assigned

to the later analyte. The result is that the area assigned to each analyte was the area between the lowest points on either side of its highest point.

This method was certain to avoid missing any area corresponding to any particular analyte, because the sum of the areas of all peaks identified by the integration tool exactly equaled the total area under the chromatogram curve. The error introduced by this method for each analyte was at most the area of the later boundary peak for each analyte. For very sharp peaks with no tail, like the one at the far left of Figure 6 above, only one peak was identified by the integration tool, and no error was introduced at all. For flat peaks or peaks with tails, like the prominent peak occupying most of Figure 6 above, the area of the boundary peak was an insignificant fraction of the total area of either the earlier or the later analyte, less than 1%.

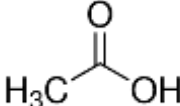
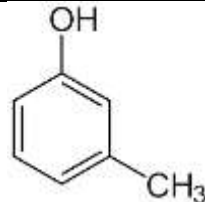

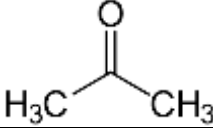
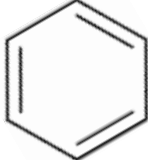
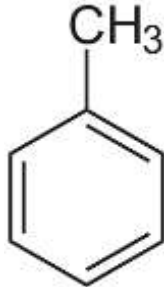
## **Experiment Design, Results, and Discussion**

### *Experiment Design Considerations*

The most practical experiment possible would be a proof of concept using real Stage 1 torrefaction product mixtures. However, the content of these mixtures depends strongly on the original feedstock. Because so many different potential feedstocks are being studied, it would be impractical to conduct separate experiments on all of them. Since activated carbon is expected to separate compounds by group, according to their interactions with the oxygenated surface groups, it makes more sense to perform experiments using representative compounds from each group. More specifically, by studying the effect of different functionalities on the

adsorptive behavior of an adsorbate, general conclusions can be drawn which apply to any torrefaction product mixture for which the content of various functionalities is known.

In order to study the effect of different functionalities on the adsorptive behavior of torrefaction products, several representative compounds were selected. Table 4 on the following page lists the representative compounds used in these adsorption experiments, and the functionalities they represent. Obviously, representative compounds cannot exactly duplicate the expected behavior of real mixture compounds, and some real mixture compounds may be too complex for their functionality to be fairly representative. However, the deviation of real mixture compounds from the behavior of representative compounds, and the concentrations of complex compounds in real mixtures, were not considered for the purposes of these experiments.

Compound	Structure Diagram	Representative Functionalities	Estimated Concentration of Rep. Functionalities in Real Stage 1 Mixtures [16]
Acetic Acid		Carboxylic acid	28% wt
<i>m</i> -Cresol		Phenolic	3%
Ethanol		Alcohol	0%-4%
Acetone		Ketone	0%-4%
Benzene		Aromatic ring	≈0%
Toluene		Aromatic ring (with steric hindrance)	≈0%

**Table 4: Representative compounds and their structures, functionalities, and concentrations**

### *Controls and Baselines*

Previous work on activated carbon adsorptive chromatography using this GC system demonstrated a need for clear, consistent procedures and controls. Significant effort was

expended developing consistent procedures for data collection and analysis using this GC system. Simple procedures for collecting control data were also developed, and control data relevant to the experimental work performed on this GC system were collected.

A control column packed with non-adsorptive glass wool was constructed. To ensure that the packing of the glass wool did not significantly alter flow rates, flow paths, flow velocities, or data collection, the control column was checked by injecting 5  $\mu\text{L}$  of methane at the flow conditions specified in the Procedures section above. A separate methane control run was conducted for each operating temperature used in experiments. The retention time and peak area were recorded. For each experimental run, the retention time and peak area of the 5  $\mu\text{L}$  methane injection were compared to this control run. Retention times within the margin of error indicated no significant difference in flow paths due to packing differences. Peak areas within the margin of error indicated no significant difference in FID response, carrier flow rate, or carrier flow velocity. No significant differences between methane control runs at different temperatures were found.

Control runs were also performed for each representative compound listed in Table 4 above. During these control runs, the standard procedure outlined in the Procedures section above was followed. The analyte for these runs was 5  $\mu\text{L}$  of a particular representative compound. A separate control run was conducted for each compound at each operating temperature used in experiments. The retention time and peak area for each representative compound were recorded. No significant differences between the behavior of methane in these control runs and the behavior of methane in the methane control runs were observed. No significant differences between control runs at different temperatures were found for any

representative compound. These control runs formed the basis against which experimental values were compared.

Table 5 on the following page shows the retention time and peak area for the control run of each representative compound, as well as methane.

### *Single-Component Chromatography Experiments*

The simplest experiments conducted were single-component runs for each compound on activated carbon. The standard procedure outlined in the Procedures section was followed for these experiments. For these experiments, a column packed with 469.3 mg of activated carbon was used. The bed length was 11.2 inches. Using a particle density of 725 mg/mL [27], the bed void fraction was 0.51. The analyte in each experiment was 5  $\mu$ L of a particular representative compound. The temperature used for these experiments was 300 °C, followed by a bakeout at 350 °C to desorb adsorbates as completely as possible.

For each representative compound, it was expected that either adsorption would occur or that it would not occur. If adsorption occurred, it was expected that the retention time would increase compared to the control. If adsorption did not occur, it was expected that the retention time would not change significantly compared to the control.

The methane compared well to the control for each experiment, indicating that the FID was operating normally and the experiments could be compared to other experiments at the

same conditions. Table 5 below shows the retention times and peak areas for each representative compound for both the control and experimental runs.

Compound	Control Ret. Time (min)	Control Peak Area (arb.)	Exper. Ret. Time (min)	Exper. Peak Area (arb.)	Ret. Time Change	Area Change
Acetic Acid	0.130	8.30 E+4	0.193	8.49 E+4	+48%	+2.3%
<i>m</i> -Cresol	0.373	1.45 E+6	3.373	6.25 E+5	+804%	-56.9%
Ethanol	0.040	2.24 E+5	0.116	2.06 E+5	+190%	-8.0%
Acetone	0.033	1.19 E+5	0.070	1.24 E+5	+112%	+4.2%
Benzene	0.036	8.71 E+5	0.516	7.66 E+5	+1330%	-12.1%
Toluene	0.040	1.94 E+6	0.488	1.75 E+6	+1120%	-9.8%

**Table 5: Control data and chromatographic experimental data**

A longer retention time compared to the control indicates that a compound interacts with the activated carbon adsorbent. A smaller peak area compared to the control indicates that the temperatures reachable by the GC oven (350 °C) were not sufficient to desorb all of a compound. The magnitude of the change in retention time corresponds to the amount and strength of interaction between the adsorbate compound and the activated carbon adsorbent. The magnitude of the change in peak area corresponds to the amount of interaction which is sufficiently strong that a temperature of 350 °C is not high enough to induce a measurable rate of desorption. Chapter 3 focuses more closely on strong interactions between adsorbate compounds and the activated carbon adsorbent surface.

As the data show, benzene and toluene interact only weakly, but are held up significantly longer when activated carbon is used as an adsorbent compared to glass wool. Ethanol, acetone and acetic acid interact with activated carbon, as evidenced by the longer hold-up time compared to glass wool, but not strongly, as evidenced by the insignificant



difference in peak area. On the other hand, *m*-cresol adsorbs readily onto activated carbon, and not all the *m*-cresol can be readily desorbed, even at 350 °C.

Because benzene and toluene have aromatic rings, whereas acetic acid, acetone, and ethanol do not, a potential interpretation of these data is that benzene and toluene adsorb using a  $\pi$ - $\pi$  stacking or other  $\pi$ -interaction mechanism, while the light oxygenates adsorb via hydrogen bonding.  $\pi$ - $\pi$  stacking is a much stronger interaction than hydrogen bonding, and occurs on flat carbon ring sites. It has been shown that unsaturated carbon ring sites exist on activated carbon [23]. Stronger adsorption means the retention time should be significantly longer and the peak area significantly smaller for aromatics in the experimental group than in the control group, which is what was observed. Conversely, a much smaller increase in retention time and decrease in peak area should be observed for the light oxygenates, which is supported by these data. At 300 °C, the equilibrium coverages of ethanol, acetone, and acetic acid are all nearly zero, while the equilibrium coverages of benzene and toluene appear relatively low – less than 15%. It is plausible that the difference in peak area between the glass wool control and the activated carbon experiment for benzene and toluene can be explained by a difference in adsorption mechanism alone. However, this explanation is not sufficient to describe the observed difference in peak area change between *m*-cresol and the other aromatics.

Because cresol contains a phenolic hydroxyl group, it is capable of hydrogen bonding with hydrogenated or oxygenated sites, such as those that exist on the surface of activated carbon. The much greater decrease in peak area for the cresol compared to the toluene and benzene indicates that the adsorption of cresol is stronger. This means less cresol can be

desorbed at 350 °C than benzene or toluene, which explains the much greater decrease in peak area. But if the adsorption of cresol is stronger than the adsorption of benzene or toluene, then the mechanism of adsorption is likely different. It is plausible that the cresol adsorbs preferentially to sites at which it can undergo both  $\pi$ - $\pi$  stacking and hydrogen bonding – that is, sites where a flat unsaturated ring site is adjacent to an oxygenated site. Hydrogen bonding between the phenolic group and the oxygenated site, alongside the  $\pi$ - $\pi$  stacking of the aromatic ring and the flat ring site, leads to a stronger interaction by the combination of two mechanisms. Quinone sites, which have been demonstrated in activated carbons by FTIR, fit the requirements for this adsorption mode perfectly [23]. Quinones have also been shown to undergo  $\pi$ -interactions readily, further contributing to the evidence for quinones as a site with which cresol would interact much more strongly than benzene or toluene [22].

The retention time of *m*-cresol in the glass wool column was significantly longer than for any other representative compound. This could have to do with poor vaporization of the liquid *m*-cresol injection, or with undesired interaction with the hypothetically non-adsorptive glass wool packing. Nevertheless, the retention time of *m*-cresol on the experimental activated carbon column was significantly longer than for the control run, or for any other representative compound on the same activated carbon column. Since *m*-cresol, the compound representing phenolics in a stage 1 torrefaction mixture, adsorbs readily onto activated carbon and is not readily removed at low temperatures, while other aromatics and light oxygenates, especially acetic acid, are readily removed even at low temperatures, activated carbon is a good choice of adsorbent for chromatographic separation of stage 1 torrefaction mixtures.

### *Multi-Component Chromatography Experiments*

Because the objective of these experiments was to provide insight into chromatographic separation processes for stage 1 torrefaction mixtures, the most useful multi-component mixture to study was acetic acid and *m*-cresol. In order to emulate a real torrefaction product mixture, and in order to follow with prior work, a binary mixture of 80% acetic acid and 20% *m*-cresol by volume was used. The same column parameters as the single-component experiments were used: 469.3 mg of activated carbon packed into an 11.2-inch column, for a packing factor of 0.51. The same carrier gas and FID supply gas flow rates and pressures were used. The same temperature of 300 °C was used, followed by a bakeout at 350 °C of the same duration. The same injection volumes of 5 µL were used, for a net volumetric content of 4 µL of acetic acid and 1 µL of *m*-cresol for each injection.

The single-component experiments discussed above comprise a useful control group for further chromatography studies on multi-component mixtures. One of the assumptions of chromatography is that a mobile-phase component will have the same retention time for the same stationary phase, regardless of changes in the composition of the mobile phase. If the retention time of a particular component in a mixture differs from the retention time of the single-component control, then that assumption is violated. An increase in the retention time of *m*-cresol, which has a longer retention time than acetic acid, would imply that the presence of acetic acid promotes the adsorption or inhibits the desorption of *m*-cresol. A decrease in the retention time of acetic acid compared to the single-component control, if accompanied by a decrease in the retention time of *m*-cresol, would imply that the two components compete for adsorption sites. An increase in the retention time of acetic acid, accompanied by a decrease in

the retention time of *m*-cresol, would imply that interactions between acetic acid and *m*-cresol both promote the adsorption of acetic acid and inhibit the adsorption of *m*-cresol. These interactions would hypothetically cause acetic acid to favor the adsorbed phase due to the presence of adsorbed *m*-cresol, and would cause *m*-cresol to favor the carrier gas phase due to the presence of acetic acid.

Formally, the four hypotheses:

1. Acetic acid promotes the adsorption or inhibits the desorption of *m*-cresol. For example, the adsorbed acetic acid is capable of hydrogen-bonding with adsorbed *m*-cresol. This adsorbate-adsorbate interaction increases the energy barrier required for *m*-cresol to desorb. The retention time of *m*-cresol increases.
2. Acetic acid and *m*-cresol compete for adsorption sites. Acetic acid and *m*-cresol both adsorb to oxygenated sites via hydrogen bonding. Because they use the same mechanism to adsorb to the same sites, they compete with each other for those sites. The retention time of acetic acid and *m*-cresol both decrease.
3. Acetic acid and *m*-cresol interact with each other, promoting the adsorption of acetic acid and inhibiting the adsorption of *m*-cresol. Acetic acid has been shown not to bind strongly to activated carbon, while *m*-cresol has been shown to bind strongly to activated carbon. However, vapor-phase acetic acid can hydrogen bond with adsorbed *m*-cresol, if the cresol is adsorbed by a different mechanism than hydrogen bonding, such as  $\pi$ - $\pi$  stacking. Similarly, vapor-phase *m*-cresol can interact via hydrogen bonding with the vapor-phase acetic acid, slightly increasing the energy barrier to leave the

vapor phase and adsorb. The retention time of acetic acid increases and the retention time of *m*-cresol decreases.

4. Acetic acid and *m*-cresol do not sufficiently interact to invalidate the chromatographic assumption that the retention time of a component is independent of the component's concentration in a mixture. The retention times of acetic acid and *m*-cresol do not significantly change. This is the null hypothesis.

The methane compared well to the control for each experiment, indicating that the FID was operating normally and the experiments could be compared to other experiments at the same conditions. The results of the experiment are presented in Table 6 below. Since only 1  $\mu$ L of *m*-cresol was used, the peak area has been normalized to 5  $\mu$ L of *m*-cresol. Similarly, only 4  $\mu$ L of acetic acid was used, and the peak area change has been normalized to 5  $\mu$ L.

Compound	Single Component Ret. Time (min)	Single Component Peak Area (arb.)	Experimental Ret. Time (min)	Experimental Peak Area (arb.)	Ret. Time Change	Peak Area Change
Acetic Acid	0.193	8.49 E+4	0.149	8.79 E+4	-22.8%	+3.5%
<i>m</i> -cresol	3.373	6.25 E+5	2.947	7.05 E+5	-12.6%	+12.8%

**Table 6: Chromatography data for acetic acid and *m*-cresol binary mixture**

The decrease in retention time for both acetic acid and *m*-cresol supports the conclusion that acetic acid and *m*-cresol compete for adsorption sites. In addition, the significant increase in *m*-cresol peak area indicates that acetic acid occupies some of the same sites to which *m*-cresol adsorbs so strongly that it cannot be removed at 350 °C. In contrast, the acetic acid peak area did not significantly change, indicating that the presence of *m*-cresol does not prevent acetic acid from desorbing.

In order to eliminate solute-solute or adsorbate-adsorbate interactions, an identical experiment was carried out, but using benzene in the place of *m*-cresol. Benzene was selected as a cresol analogue without the hydroxyl functionality, to minimize the amount of favorable interaction between it and acetic acid via hydrogen bonding. The sample mixture, therefore, was 80% acetic acid and 20% benzene by volume, for an injection volume of 4  $\mu$ L acetic acid and 1  $\mu$ L benzene. An identical column and temperature program to the acetic acid – *m*-cresol binary mixture experiment were used.

The methane compared well to the control for each experiment, indicating that the FID was operating normally and the experiments could be compared to other experiments at the same conditions. The results of the experiment are presented in Table 7 below. Peak area values have been normalized to 5  $\mu$ L.

Compound	Retention Time (min)	Peak Area (arb.)	RT Change over Single	Area Change over Single	RT Change over Cresol Binary	Area Change over Cresol Binary
Acetic Acid	0.195	8.49 E+4	+1.0%	+0.0%	+30.9%	-3.4%
Benzene	0.606	7.82 E+5	+17.4%	+2.1%	N/A	N/A

**Table 7: Chromatography data for acetic acid and benzene binary mixture**

In the acetic acid-benzene binary mixture, no significant difference was observed between the acetic acid residence time and the acetic acid single-component residence time. No difference was observed between the acetic acid peak area and the single-component acetic acid peak area. This indicates that benzene does not block sites at which acetic acid adsorbs, like cresol does. However, this experiment could not rule out the possibility that solute-solute or adsorbate-adsorbate interactions affect the retention time of acetic acid in a mixture with *m*-cresol. Interestingly, the retention time of benzene increased in the mixture with acetic acid,

compared to the retention time of benzene by itself. This suggests that the presence of acetic acid helps to promote the adsorption of benzene on activated carbon. A possible mechanism for this promotion effect is that acetic acid hydrogen-bonds to an oxygenated site on the activated carbon surface, which reduces the repulsion between the electron-rich aromatic ring and the electron-rich oxygenated surface, thereby increasing the likelihood of adsorption and increasing the retention time of benzene. Although it seems that this should result in a decreased peak area for acetic acid, it has been shown above that acetic acid does not remain adsorbed to activated carbon indefinitely at 300 °C. It remains on the surface only long enough to marginally increase the likelihood of adsorption of benzene, and therefore marginally more benzene adsorbs than would adsorb without the presence of acetic acid.

These results seem to discount the possibility of an acetic acid-catalyzed oligomerization reaction occurring, wherein *m*-cresol units couple using an esterification reaction, for example. Such a reaction would lead to decreased peak area for *m*-cresol when fed along with acetic acid, because either the oligomers would condense out of the vapor phase at the temperatures involved in these experiments, or they would cause the concentration of organics in the effluent to decrease relative to an equivalent mass of *m*-cresol alone, and therefore the FID signal would decrease. Because the peak area of *m*-cresol increases instead, it is unlikely that such a reaction is occurring. Further work should investigate this phenomenon using a Parr reactor with an in-line mass spectrometer, to confirm the chemical identity of the effluent organics.

## *Column Length Chromatography Experiments*

Chromatographic separation depends on a relatively long contact time between the mobile phase and the stationary phase. Due to the limitations of the apparatus available, it was infeasible to change the length of stainless steel tubing used to house the adsorbent material. Therefore, to investigate the effects of column length on separation, the length of the adsorbent bed within the stainless steel tubing was shortened. 186.9 mg of activated carbon was packed into 4.5 in of column, for a packing factor of 0.506. As noted in the apparatus section above, the upstream glass wool plug was inserted further into the column, to prevent activated carbon adsorbent from shifting or spilling during use. The same 80% acetic acid, 20% *m*-cresol by volume mixture was used, for a total injection volume of 4  $\mu\text{L}$  of acetic acid and 1  $\mu\text{L}$  of *m*-cresol. The same temperature of 300 °C and the same 350 °C bakeout duration were used. The same FID supply gas flow rates were used. The upstream pressure of the carrier gas had to be adjusted. Because the column was packed with less material than the standard column, the pressure drop due to the packed bed was lower. This meant a smaller pressure driving force was needed to achieve the same flow rate. In addition, the frequency of FID flame outages using the shorter column was unusually high compared to the frequency of FID flame outages using the standard column, as long as the same carrier gas flow rate was used. A lower flow rate of 100 mL/min (compared to 150 mL/min on the standard column) was used instead to avoid FID flame outages.

Because the adsorbent bed length was decreased by a greater percentage (-59.8%) than the carrier gas flow rate (-33.3%), the contact time should still decrease. Shortening the length



of the bed should also change the total capacity available for adsorption which is not easily reversible at 350 °C. Capacity is discussed more thoroughly in Chapter 3 below.

The methane compared well to the control for each experiment, indicating that the FID was operating normally and the peak area could be compared to other experiments at the same temperature conditions. The results of the experiment are presented in Table 8 below.

Peak area values have been normalized to 5  $\mu$ L.

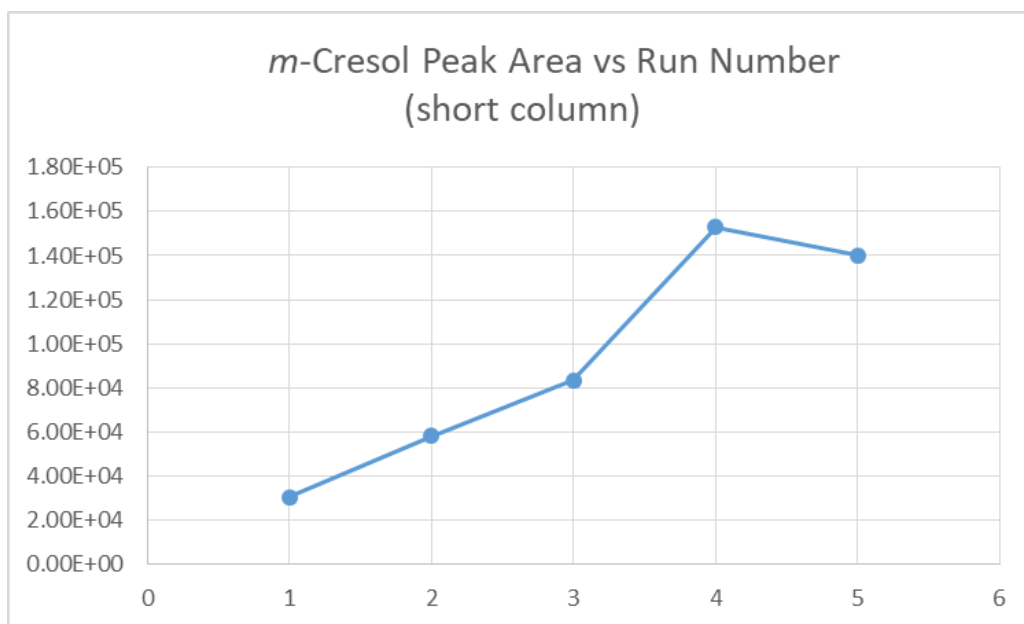
Compound	Short Ret. Time (min)	Short Peak Area (arb.)	Std. Ret. Time (min)	Std. Peak Area (arb.)	Ret. Time Change	Peak Area Change
Acetic Acid	0.113	1.17 E+5	0.193	8.49 E+4	-41.5%	+37.8%
<i>m</i> -Cresol	13.883	7.00 E+5	3.373	6.25 E+5	+311.6%	+12.0%

**Table 8: Short column chromatography data**

The peak area of both compounds is greater for the shorter column than for the standard length column. This is good evidence for the hypothesis that all compounds adsorb irreversibly to some extent. However, it must be noted that due to the carrier gas flow rate difference, the results of experiments on the short column should not be treated as comparable to the results of experiments on the standard column. In particular, the retention time of *m*-cresol was significantly longer for the short column than for the standard length column. This contradicts the expectation that a shorter column should result in a shorter retention time. It is likely that the lower carrier gas flow rate is the primary reason for the unusually long retention time of *m*-cresol. However, it is also possible that the empty space of several inches at the beginning of the column contributed to the longer retention time. In either case, experiments on the short column should not be compared to experiments on the standard length column.

Creating a new column is a time-consuming process, involving cutting a tube to length, tapering the tube ends, careful packing of adsorbent material, and calibration of supply gas flow rates. In addition, if the flow patterns of the new column cause the FID flame to go out, the column must be rejected and rebuilt. For these reasons, and because it was not possible to build a short column such that the same carrier gas parameters could be used, further experimentation with column length was not pursued.

During the experimentation on the short column, however, a trend was discovered which related to the peak areas recorded on individual runs. A graph of *m*-cresol peak area vs run number is presented in Figure 7 below. Between the first recorded run and the fourth recorded run, the *m*-cresol peak area increased by a factor of 5. It was hypothesized that this increase in peak area was due to the permanent occupation of adsorption sites by *m*-cresol molecules. Chapter 3 discusses the investigation of activated carbon adsorption capacity and capacity loss as a result of adsorption which cannot be reversed at low temperatures.



**Figure 8: Change in *m*-cresol peak area with number of runs**

## Chapter 3: Adsorptive Capacity and Capacity Loss Experiments

### Experimental Apparatus

#### *GC Apparatus*

The same GC apparatus was used as in the chromatography experiments in Chapter 2. A standard column was used, with length 10.5 inches of carbon packing, weighing 458.5 mg, for a packing factor of 0.499.

#### *TGA/DSC Apparatus*

A Netzsch STA 449 F1 Jupiter Simultaneous Thermal Analyzer was used to conduct thermogravimetric desorption and differential scanning calorimetry studies. The sample crucible was loaded with adsorbent material, and then pulses of adsorbate at normal vapor pressures were passed over the crucible and adsorbent material. Pulses were collected in a sample loop, which had a constant flow rate of carrier gas through it. The carrier gas was bubbled through a liquid sample contained in a sealed flask, then through the sample loop and out a vent. In this manner, a repeatable concentration of adsorbate could be collected in the sample loop for injection. It was assumed that this concentration was equal to the vapor pressure of the adsorbate gas. Upon injection, the carrier gas was re-routed from the sample loop to the experimental chamber, instead of directly to the vent. The carrier gas used to collect the sample was argon. The adsorption of adsorbate onto the adsorbent increased the total mass of the crucible and sample, which was detected to a high degree of precision by the

machine. The adsorption process also released an amount of heat equal to the enthalpy of adsorption, which was measured by measuring the change in the amount of energy required to keep the sample and crucible at a constant temperature. Based on the formula weight of the adsorbate, it was possible to calculate both the adsorption capacity at a certain temperature, and the molar or specific enthalpy of adsorption at that temperature. Special thanks to Lawrence Barrett, who operated and maintained the machine.

## **Experimental Procedure and Data Analysis**

### *GC Procedure and Analysis*

The same procedure and analysis methods were used for adsorption capacity experiments conducted using the GC column and FID as were used for chromatography experiments using the GC column and FID.

### *TGA/DSC Procedure and Analysis*

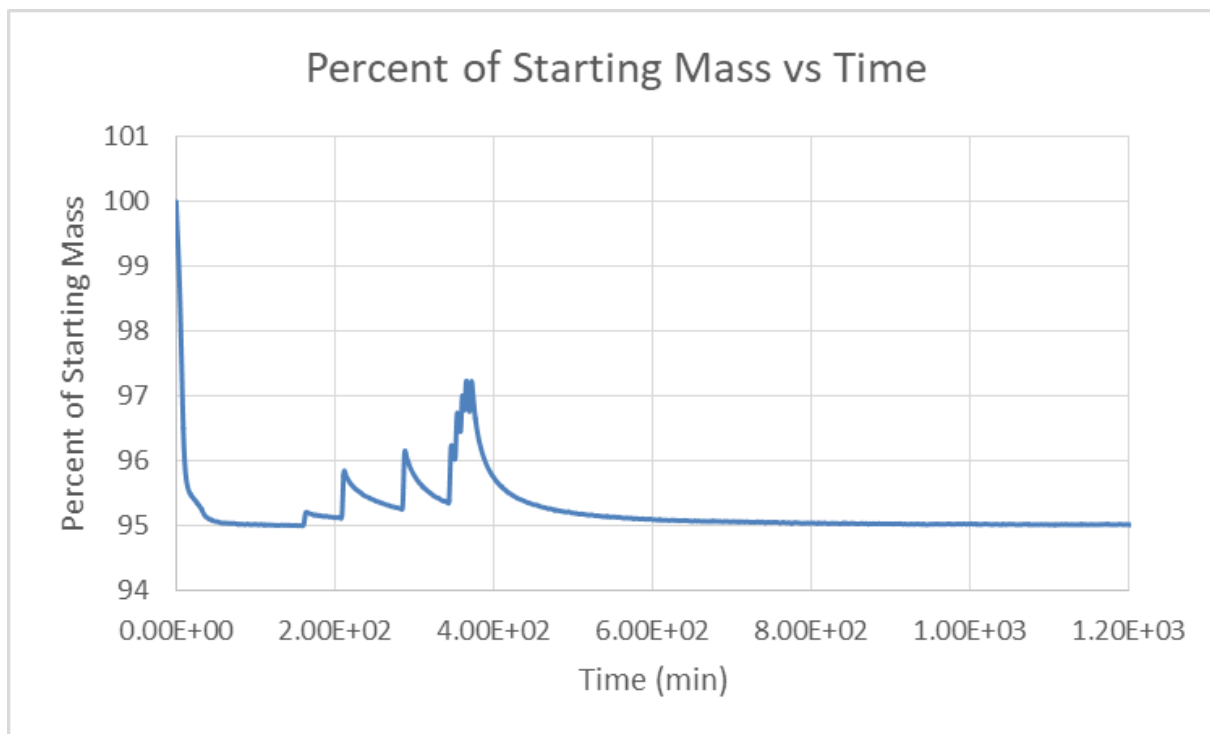
A constant temperature of 250 °C was used for all TGA/DSC experiments. Pulses of sample were performed every 10 to 30 minutes, depending on the time it took the mass reading to reach a steady value. A low flow rate of carrier gas was used to ensure that the partial pressure of the sample contacting the adsorbent was equal to the vapor pressure of the gas in the sample flask. Depending on the adsorption capacity for the particular representative

compound and the adsorption rates near maximum capacity, anywhere from 5 to 50 pulses were performed.

When a run was finished, two categories of data had been collected: mass data and energy data. For each pulse, the mass reading increased from its starting value, then decreased to a steady value as material contacted the adsorbent and then was driven off. The mass change from the starting value to the steady value was recorded. Once the difference between the starting value and the steady value was negligible, the run was terminated. The total change in mass between the initial starting value and the final steady value was recorded, and the adsorption capacity was calculated in units of g/g.

The amount of energy being added to the system by the built-in temperature controller to maintain its temperature was constantly measured and compared to a reference value. Note that the controller added energy to the system while no adsorption was occurring, because small amounts of energy were lost to the environment. While adsorption was occurring, the heat released by the adsorption process caused the amount of energy added to maintain a constant temperature to decrease. For each pulse, that amount of energy decreased from its starting value and then increased again back to its starting value, representing an energy release from the adsorption process. Because it is possible to calculate the amount adsorbed per pulse, it is also possible to calculate from the energy data the heat of adsorption. However, the energy measurement must be calibrated separately for each sample. The calibration process is difficult and time-consuming, and it was determined that it would not be possible to measure the heat of adsorption during every run.

Figure 8 below shows a typical TGA plot of the mass measurement vs time. The mass is reported as a percentage of the mass measured by the scale at the start of the run, which was recorded separately in mg. The start mass recorded in Table 10 below represents the mass after incidental adsorption of water due to humidity is reversed, represented by the sharp drop during the first 60-120 minutes of the run. For this run, the start mass was recorded at time  $t = 180$  min. For each pulse, the end mass was recorded just before the mass reading began to increase for the next pulse. The final mass reading was recorded as the value approached at the end of the run, or 1200 min. The equilibrium adsorptive capacity is the difference between the final mass reading and the start mass recorded just before the first pulse. Figure 8 is the plot recorded for the adsorption of benzene.



**Figure 9: Typical TGA plot**

## Experiment Design, Results, and Discussion

### *TGA/DSC Experiments*

The first experiments conducted in the TGA/DSC apparatus were standard capacity tests for adsorptive materials. Four samples of 20-40 mesh activated carbon were prepared, which are described in Table 9 below. The procedure for preparing samples 1 and 2 involved injecting a mixture of acetic acid and *m*-cresol onto the column repeatedly at 350 °C, until no change in peak area or retention time was observed between consecutive runs. It was assumed that this procedure resulted in carbon at its equilibrium adsorptive capacity for *m*-cresol and acetic acid at 350 °C. Heat treatment refers to holding the activated carbon isothermal at 500 °C for 24 hours prior to TGA/DSC experimentation, which was intended to promote desorption of adsorbates even from sites from which they could not be desorbed at 350 °C. Manufacture date was varied to investigate whether adsorptive capacity degraded naturally over time.

<b>Sample</b>	<b>Manufacture Year</b>	<b>Usage Status</b>	<b>Heat Treatment</b>
1	2012	Used	Treated
2	2012	Used	Untreated
3	2012	Fresh	Untreated
4	2017	Fresh	Untreated

**Table 9: Carbon sample numbers and descriptions**

Each sample was subjected to pulses of isopropylamine (IPA) according to the procedure outlined above. These experiments were intended to investigate the diversity of active sites to which adsorbates can adsorb on activated carbon, and the circumstances under which the adsorptive capacity of these sites can diminish. IPA was selected as the adsorbent because it has been shown to adsorb readily to Brønsted acid sites [28, 29]. It was expected based on

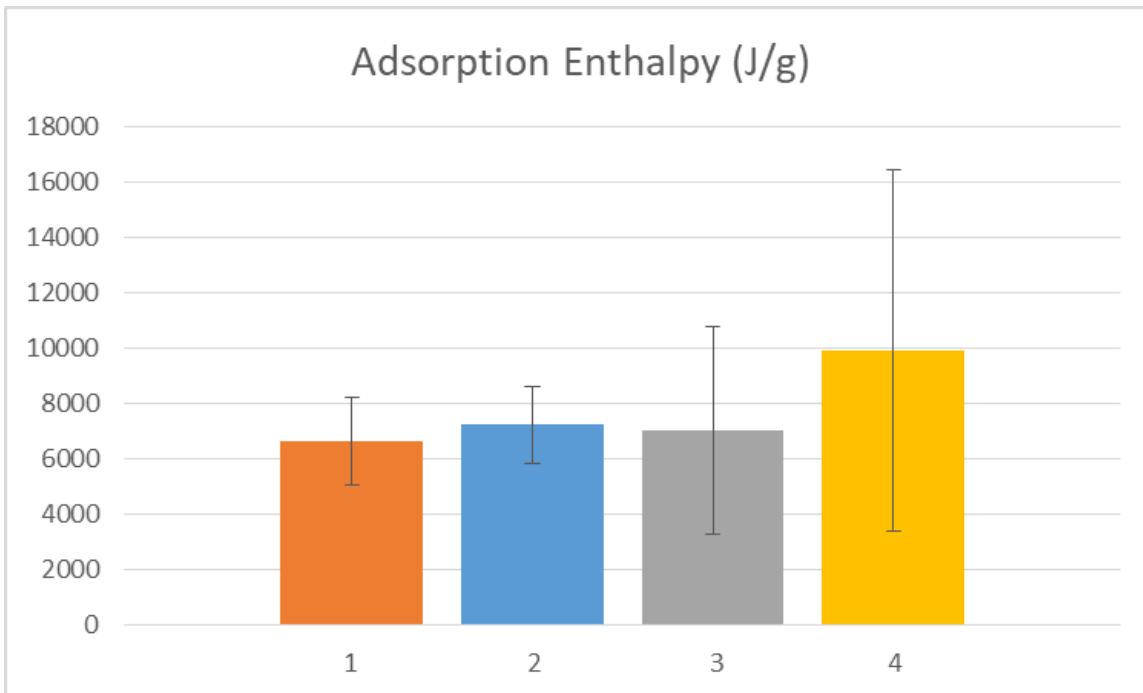
previous work that the oxygenated sites on activated carbon include Brønsted acid sites like carboxylic acid sites and phenolic sites; however, the literature also noted that common types of oxygenated sites on activated carbon include heterocycles like pyrenes and chromenes [23]. Heterocyclic oxygenated sites would not interact strongly with IPA, and so they would not be accounted for using this experimental method. On the other hand, heterocyclic oxygenated sites are only very rarely found at edge and corner positions, making their availability for adsorption small compared to acid sites [23]. Based on data from the literature using methane as an adsorbate on activated carbon monolith adsorbents, 161 g per kg carbon total capacity at room temperature is expected [30].

Table 10 below displays the results of these experiments. Figure 9 on the following page presents the adsorption enthalpy data in graphical form, including error bars.

<b>Sample</b>	<b>Start Mass (mg)</b>	<b>Added Mass (mg)</b>	<b>IPA Adsorptive Capacity (g/g)</b>	<b>Adsorption Enthalpy (J/g)</b>
1	25.43083	0.363225	0.0143	6600
2	23.98152	0.068325	0.00285	7200
3	36.09453	1.061388	0.0294	7000
4	19.68061	0.5414236	0.0275	9900

**Table 10: TGA/DSC data for IPA on several carbon samples**





**Figure 10: Adsorption enthalpy for carbon samples via TGA/DSC**

A very low adsorptive capacity was observed for sample 2, a larger capacity was observed for sample 1, and the largest capacity was observed for samples 3 and 4. These results support the hypothesis that a broad variety of sites on activated carbon should result in a gradient of adsorptive strengths. Because of the variability of adsorptive strength, cresol desorbed from some sites at 350 °C, because the relatively low temperature was sufficient to overcome energy barriers for desorption which were relatively small. When the temperature was increased to 500 °C for heat treatment, cresol desorbed from further sites, because the higher temperature was sufficient to overcome larger energy barriers for desorption. But even at 500 °C, not all of the adsorbed material could be desorbed, because some sites allow for very strong adsorption, for which the desorption energy barrier could not be overcome at 500 °C.

A reasonable conclusion from these results is that a broad variety of active sites exist on activated carbon, that the primary mechanism of capacity loss is permanent adsorption, and that some of the “permanent” adsorption can be reversed with sufficiently high temperature. This conclusion is a favorable one for prospective adsorptive separation processes in which recovery of the adsorbed phenolics is desirable. If a large fraction of the adsorptive capacity can be regenerated with sufficiently high temperature, and a large fraction of the adsorbed phenolics can be selectively recovered, then the largest challenge remaining for the design of such a process is to find the optimum temperatures for the adsorption and desorption stages. However, no attempt was made to identify the volatiles released by the used sample during heat treatment. It is possible that the activated carbon catalyzed a reaction of some kind, and that the compounds which do not desorb at 350 °C but do desorb at 500 °C are not *m*-cresol, but a reaction product. Further work is needed to identify the compounds released during heat treatment.

The adsorption enthalpy data also support the conclusion of a broad variety of active sites, but also raise further questions. First, the greatest adsorption enthalpy is for the recently manufactured, fresh carbon. This suggests that the strongest sites are available on recently manufactured activated carbon which has not been used for adsorption. However, it also suggests that the recency of manufacture plays a role in the strength of active sites. This leads to a conclusion which is difficult to reconcile with the conclusion drawn from the adsorptive capacity data. If the strength of active sites diminishes over time at room temperature, but the adsorptive capacity is not significantly changed over time, then it is plausible that the identity of the active sites changes over time, with highly reactive oxygenated surface sites decaying into

less reactive, but more stable oxygenated surface sites. Further work is needed to investigate this hypothesis.

In addition, the uncertainty in the measurements of adsorption enthalpy is very large compared to the enthalpy values. The enthalpy values were calculated individually for each pulse of isopropylamine adsorbate. The mass change from each pulse was measured, indicating the mass of isopropylamine which had adsorbed during that pulse. The area inside the curve showing heater power was found for each pulse, which was the total amount of energy released by the adsorption during that pulse. Dividing the total amount of energy released in a particular pulse by the mass increase during that same pulse yielded an adsorption enthalpy value for each pulse. Because many pulses were conducted for each run, each of which was at the same temperature and the same concentration and amount of adsorbate, the average adsorption enthalpy for each sample was found and reported, and the standard deviation was recorded as the uncertainty.

Second, the capacity observed is much lower than literature values. The study on methane reported 161 g/kg, which is the equivalent of about 10.1 mol/kg. The highest capacity observed in this work was 29.4 g/kg, which is the equivalent of about 0.50 mol/kg. The discrepancy between the observed molar capacity and the literature molar capacity is likely because the experiments were conducted at different temperatures; the literature value was recorded at room temperature, and the value from these experiments was recorded at 250 °C. It is also possible that the discrepancy is observed because methane and isopropylamine do not adsorb to the same sites. It has been shown that isopropylamine adsorbs readily to Brønsted acid sites, but some sites on the activated carbon surface may be Lewis acid or base sites, which

would explain their interaction with the representative compounds of interest. Another possible explanation is that isopropylamine cannot access sites within pores too small for it to travel through, while methane is small enough to access those sites. This work was not intended to replicate the values found in the published literature, but further work should attempt to reconcile the difference between this work and prior work.

Third, there is no significant difference between the adsorption enthalpies on fresh or used old carbon. Unfortunately, no used samples of new carbon were available during the time allotted to this project for use of the TGA/DSC machine. Further work is needed to investigate whether the adsorption enthalpy depends only on the age of the carbon, or whether it also depends on the occupancy of the strongest adsorption sites.

Another set of experiments was performed which investigated the adsorptive capacity of representative compounds on activated carbon. With the time available on the TGA/DSC equipment, it was not feasible to conduct DSC for this set of experiments, so the heats of adsorption of the different representative compounds could not be measured. The same procedure as for IPA adsorption was used for all compounds, including the temperature of 250 °C. The activated carbon sample used was new fresh carbon for all experiments in this set. Table 11 on the following page presents the results of this set of experiments. Acetone was not finished in the time available on the TGA/DSC equipment.

Compound	Start Mass (mg)	Added Mass (mg)	Adsorptive Capacity (g/g)
Acetic Acid	24.3783	0.0055266	0.000227
Ethanol	22.2672	0.0451044	0.002026
Benzene	26.477	0.0553581	0.002091
Toluene	26.2988	0.3875542	0.014737
<i>m</i> -cresol	19.649	0.4831434	0.024589

**Table 11: TGA adsorption data for several representative compounds**

As expected, the equilibrium adsorptive capacity at 250 °C was small for the light oxygenates and for benzene, and very large for the *m*-cresol. The equilibrium adsorptive capacity at 250 °C was also surprisingly large for toluene. Further work is recommended to investigate toluene specifically.

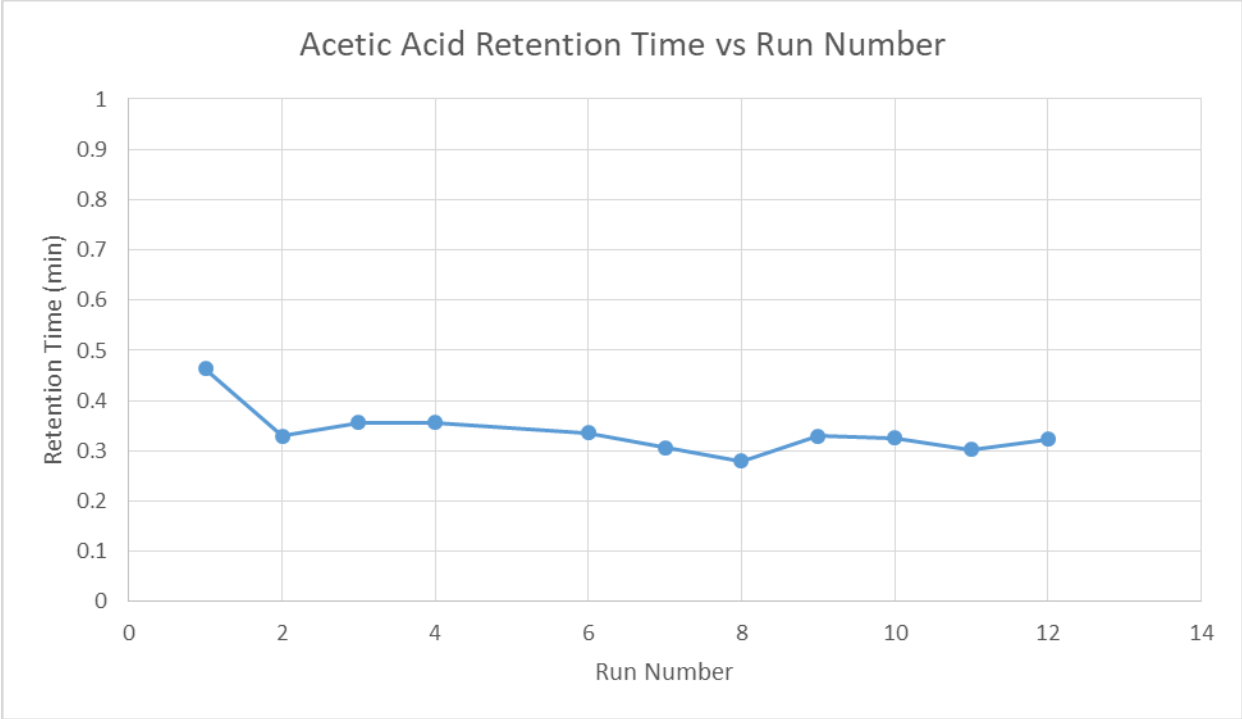
### *GC Experiments*

To supplement the TGA/DSC data, and to examine how the adsorptive capacity of an activated carbon adsorbent bed changes over time, experiments were carried out on the same GC setup as for the chromatography experiments in Chapter 2. The conditions of interest for a real biofuels mixture do not involve passing pure cresol over a bed of activated carbon. Because it is likely that competition from acetic acid decreases the rate at which cresol can permanently occupy sites, the same mixture composition was used for these capacity experiments as was used for the earlier chromatography experiments.

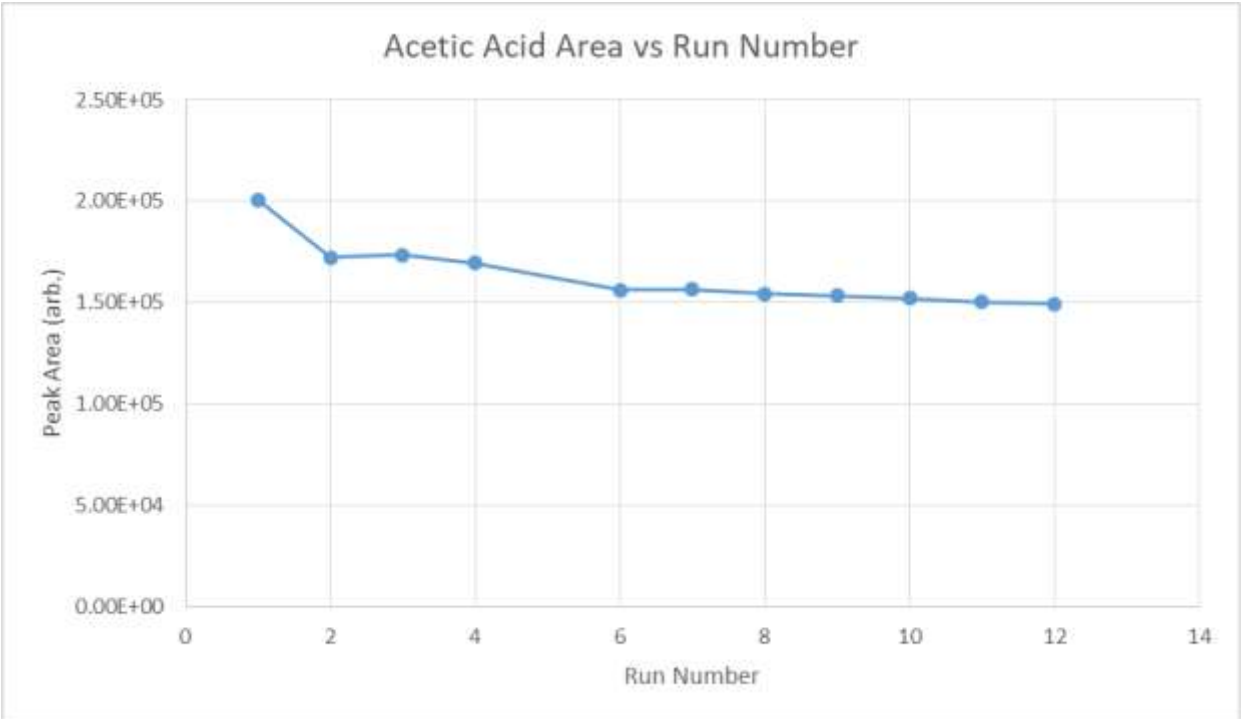
Mixtures of 80% acetic acid and 20% *m*-cresol by volume were injected in volumes of 5  $\mu$ L, for a total injection volume of 4  $\mu$ L of acetic acid and 1  $\mu$ L of *m*-cresol. A fresh adsorbent

bed was prepared with the specifications outlined in the apparatus section of this chapter. A temperature program was created which held the bed at 250 °C for 200 minutes, and then conducted a bakeout at 350 °C for 100 minutes. Prior work had determined that for a bed of similar size and injections of similar composition and size, this temperature program would capture all adsorbate leaving the column during the run portion, and then would capture all desorbed material leaving the column during the bakeout portion. No *m*-cresol was eluted during the run portion at 250 °C, likely because there was not sufficient *m*-cresol loaded onto the column to saturate the sites available for adsorption at 250 °C. Because of the experiments described in this chapter above, which demonstrated that acetic acid does not remain significantly adsorbed to activated carbon at 250 °C, it was assumed that all material captured during the bakeout portion was *m*-cresol.

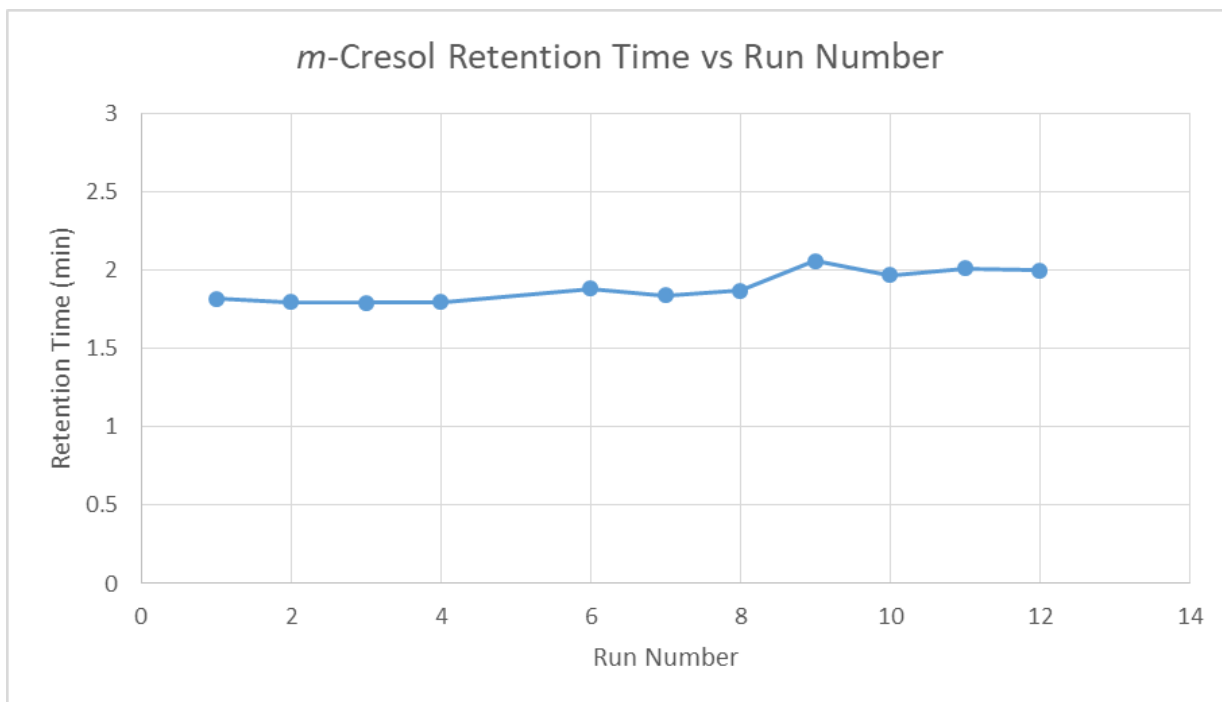
Injections were conducted 12 times sequentially. The retention times and peak areas for acetic acid and *m*-cresol are presented in Figures 10-13 on the following pages. Note that data point 5 is absent; this is because an abnormal flow pattern caused the FID to read improperly, but the adsorbate material still travelled through the column normally, so the run must count toward the total amounts injected.



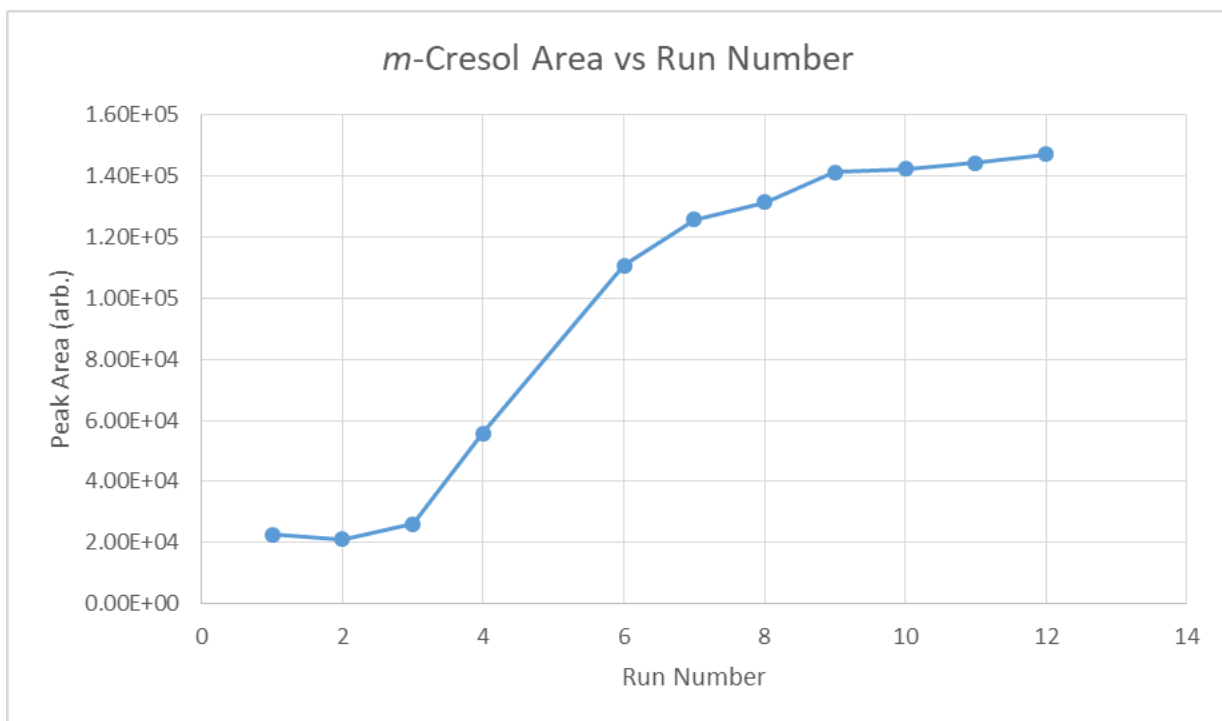
**Figure 11: Change in acetic acid retention time with number of runs**



**Figure 12: Change in acetic acid peak area with number of runs**



**Figure 13: Change in *m*-cresol retention time with number of runs**



**Figure 14: Change in *m*-cresol peak area with number of runs**



The retention time and peak area of acetic acid decrease relatively slowly with number of runs. Meanwhile, the retention time of *m*-cresol increases slowly with number of runs, while the peak area of *m*-cresol displays a characteristic breakthrough curve. The peak area increases by a factor of 7 from the earliest runs to the latest, indicating an average of around 86% uptake on a fresh column and near 0% uptake on a thoroughly used column. Around 3  $\mu\text{L}$  of *m*-cresol are injected before capacity loss significantly begins, and around 9  $\mu\text{L}$  are injected before the significant majority of capacity is lost. The control experiments from Chapter 2 provide a good comparison for the FID signal to be expected from a given volume of *m*-cresol. If it is assumed that the FID signal associated with 5  $\mu\text{L}$  of *m*-cresol is given by the glass wool chromatography experiments in Chapter 2, then the adsorptive capacity of activated carbon for *m*-cresol is 0.0120 g/g, using the trapezoid rule to integrate the breakthrough curve. This value does not compare well with the value of 0.0246 g/g found using TGA/DSC. However, it is of the same order of magnitude. It is plausible that, were these capacity loss experiments continued for a longer duration, additional capacity would be lost until the value more closely approximated that found using TGA/DSC. Another plausible explanation for the difference in capacity between the TGA/DSC and the bed adsorption experiments is that the cresol reacted to form a dimer. Because the FID signal depends only on the concentration of organic species in the effluent gas, a volatile dimer would produce only half the signal. However, it is also unlikely that 100% of the cresol was converted into a dimer, with no further oligomerization occurring.

## Industrial-Scale Temperature-Swing Adsorption Process Design

With the capacity data from TG experiments and GC experiments, it is possible to design a hypothetical scaled-up adsorption process using activated carbon to separate phenolic components from stage 1 torrefaction mixtures. Since the two sets of experiments arrived at different numbers for phenolic capacity, and the torrefaction of different kinds of biomass produces different stage 1 product compositions, an upper-bound and a lower-bound case were designed, as well as several intermediate cases.

A multitude of considerations were made for the purposes of this hypothetical process design. First, an initial feed of 2000 metric tons/day of raw woody biomass was chosen as an appropriate amount. Then, it was assumed that all the water mass was driven out in a drying stage prior to the torrefaction stage. A liquid yield of 13% to 33% by mass of the solid entering the torrefaction stage was assumed, based on previous studies, and depending on the type of biomass, the temperature of torrefaction, and the residence time of the dried biomass in the torrefaction unit. Phenolic content of the liquid stage 1 torrefaction product was assumed to be between 8% and 12% by mass, according to previous studies. The capacity of activated carbon for phenolics was assumed to be at a minimum, the capacity measured in the TG experiments above (6.16 g/kg), and at a maximum, the highest capacity found in literature for any adsorbate on activated carbon at any temperature (200 g/kg). The adsorption temperature selected for this process was 423.15 K, in order to minimize heat losses from the torrefaction stage while also ensuring that the process stream was vapor-phase and adsorption was possible.

The adsorption process design included several beds, most of which were to be regenerated at high temperature while the active bed underwent adsorption of phenolics out of the process stream. Because a range of process conditions were included in this design, the number of beds required depended on the conditions selected, from a minimum of three beds under optimal conditions to 100 beds under the worst case considered. It was found that the number of beds required depended on how much time was needed to remove the adsorbed phenolics from the bed, compared to the amount of time the bed could remain on-stream before being depleted. It was assumed that the equilibrium so strongly favored adsorption of phenolics that 100% of the phenolic content of the product stream was adsorbed while the bed was not depleted. It was also assumed that the breakthrough curve was very sharp relative to the size of the bed; that is, that nearly 100% of the capacity of the bed was occupied before the phenolic concentration of the effluent began to rise from zero. With these assumptions, the amount of time required to deplete a bed with a certain mass of carbon could be calculated directly.

For desorption, the kinetics developed in Chapter 2 above were used. Several candidate temperatures for desorption were selected, and the time required to desorb 99.9% of the phenolics was found for each temperature and for each bed design case selected. In addition, the time required to heat the beds to desorption temperature and cool them back to adsorption temperature were found. Even at the lowest desorption temperatures selected and for the largest adsorption capacities per gram of adsorbent, the total time required for temperature change was 74% of the total time for a desorption cycle. This means that the primary obstacle to decreasing number of beds required was heat transfer rate. If a reliable,

cheap method could be devised which cooled an adsorbent bed faster than a room-temperature inert purge gas, then the number of beds required could be substantially decreased.

However, the number of beds required was independent of the size of the beds. Because the time required to deplete a bed and the time required to heat and cool a bed were both assumed to scale linearly with temperature, the only significant changes involved in using a larger bed were longer cycle times and more up-front investment required. In fact, if the valves directing flow and the heat transfer operations can be rapidly controlled, a short cycle time would be desirable over a long cycle time because the size of bed required would decrease. In reality, very small beds would be shorn apart by the large flow rates of stage 1 products being treated, while very large beds would have even slower heat transfer rates than assumed here. Without more in-depth engineering analysis, an optimal bed size cannot be uniquely determined. For the purposes of this hypothetical process design, a bed size of 1000 kg of activated carbon was selected.

Based on the upper and lower bounds of process conditions outlined already, and the feed rate selected, Table 12 below shows the upper and lower bounds of various other process conditions.

<b>Bound</b>	<b>Stage 1 Flow (kg/s)</b>	<b>Phenolic Flow (kg/s)</b>	<b>Desorption Temperature (K)</b>	<b>Depletion Rate (kg/s)</b>	<b>Depletion Time (s)</b>
Upper	7.69	0.922	573.15	34.2	844
Lower	2.96	0.237	473.15	1.19	29.3

**Table 12: Process condition upper and lower bounds**

Table 13 below shows each of the cases examined, including the various parameter assumptions, and shows the number of beds required based on the upper and lower bound of depletion time listed in Table 12 on the previous page.

Case	$k_d^0$ (kg*s/kg)	Desorption T (K)	Capacity (kg/kg)	Regeneration Time (s)	Minimum Beds	Maximum Beds
A	0.0608	573.15	0.2	2846	5	99
B	0.000876	573.15	0.00616	2872	5	100
C	0.0608	523.15	0.2	2256	4	79
D	0.000876	523.15	0.00616	2351	4	82
E	0.0608	473.15	0.2	1453	3	51
F	0.000876	473.15	0.00616	1892	4	66

**Table 13: Process parameters for various cases**

Unsurprisingly, the minimum number of beds required came when the maximum capacity was assumed. Since the regeneration time for all cases was dominated by the heat transfer time, the lowest desorption temperature cases resulted in the fastest regeneration cycle times because less change in temperature was required. Case E combined the largest capacity assumption with the lowest desorption temperature assumption, and therefore resulted in the fewest beds required for the minimum and maximum cases. Because the desorption temperature was so low and the rate of desorption so slow, case F resulted in the longest desorption time of 492 seconds, about 26% of the total regeneration cycle time.

However, there are a few problems with case E. First, the desorption temperature is below the boiling point of several phenolics. Desorption would be much slower unless the partial pressure is kept very low, either by partial vacuum or by increasing the flow of heated, inert purge gas to carry away the desorbed phenolics faster. It is likely that the regeneration cycle time would increase due to these inefficiencies, to the point that the number of beds

required may exceed cases at higher temperatures or lower capacities. Second, it is unlikely that the conditions required for case E would be met by a real process. The capacity is unlikely to be as large as case E requires, and the depletion time is likely to be shorter than the time required to use only three beds.

To produce a more realistic process design, further assumptions were made with the information gained in the analysis of these cases, to create a case with good design choices where possible and reasonable assumptions where applicable; that is, choices that result in fewer beds, lower utility requirements, and other conditions that lead to favorable process economics. Since the conditions of torrefaction generally dictate the amount of stage 1 products produced, as well as their composition, a 15% by mass conversion to stage 1 products from dry biomass was selected. Minimizing the mass of stage 1 products to be treated helped minimize the number of beds required. It was assumed that the phenolic content of this mixture was 10.4% by mass, in accordance with the data obtained by previous work [16]. In addition, the low capacity estimate of 0.00616 kg/kg was used, as the capacity had only a small effect on the number of beds required compared to the composition and flow rate of stage 1 products. This yielded a depletion time of 74.8 seconds. A desorption temperature of 483.15 K was selected, because this temperature is slightly higher than the boiling point of cresol, the compound used to model phenolics in this work. As discussed above, the lowest possible temperature which avoids introducing other problems is desirable for the desorption process, in order to minimize heating and cooling times. In order to address potential future improvements to the torrefaction process, in which the concentration of phenolics might be reducible to a lower target of 8% by mass of the stage 1 product, while maintaining the stage 1

yield of 15% by mass of the dry biomass feed, the calculations were re-run using 8% instead of 10.4%, and presented as another case.

These cases are summarized in Table 14 below.

Case	Phenolic Content	Capacity (kg/kg)	T <sub>des</sub> (K)	Depletion Time (s)	Desorption Time (s)	Heat/Cool Time (s)	Regen Cycle Time (s)	Beds
G	10.4%	0.00616	483.15	74.8	352.95	1598	1952	28
H	8.0%	0.00616	483.15	97.2	352.95	1598	1952	22

**Table 14: Cases with torrefaction parameters advantageous for separations**

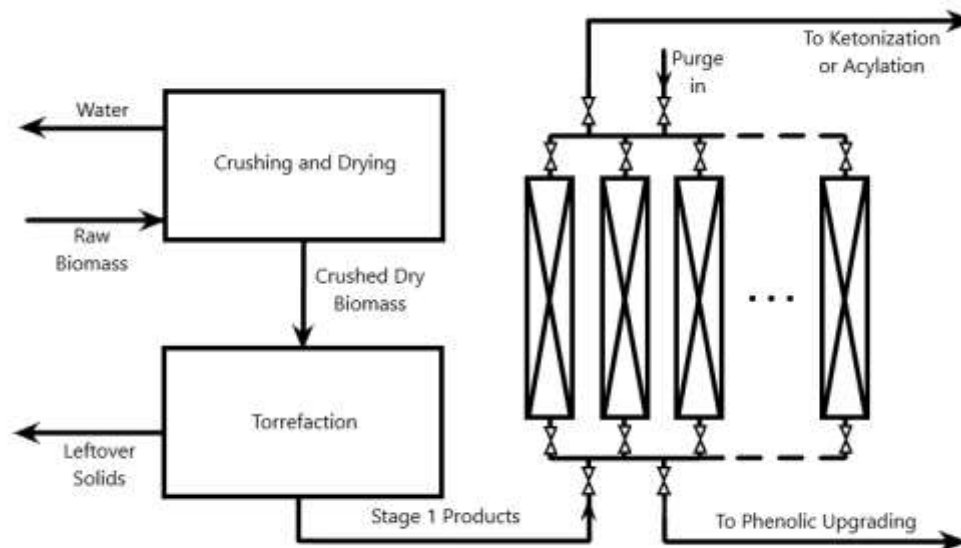
Note that the only change caused by changing the phenolic content was in the depletion time; because the bed is the same size, it has the same amount of adsorbed material when fully depleted. However, the longer time to deplete the bed means that fewer beds are needed. 22 beds still seems unusually large for even an industrial desorption process, so an estimate of bed dimensions was made. Based on bed void fractions measured in this work, a bed void fraction of 0.50 was selected. A particle diameter of 595 microns, which corresponds to 30 mesh, was also selected based on experiments in this work. A particle density of 725 kg/m<sup>3</sup> was used based on literature values [27]. Based on the composition of the stage 1 product mixture, the vapor density was estimated at 4.6 kg/m<sup>3</sup> and the viscosity at 1.0 cP (0.001 Pa\*s). Finally, a target pressure drop of approximately 400 kPa was selected, which was about twice as large as the carrier gas pressure drop for these experiments. A larger pressure drop tolerance would allow for a longer, thinner bed, but would also increase the shear stresses on the bed walls and would change the adsorption rates of phenolics at different bed coordinates. The Ergun equation was used to size the adsorption beds, based on the volume requirement and the pressure drop.

Because both cases above, G and H, involve the same mass flow rate of stage 1 products, the beds will be the same size for both cases. The results of the adsorption bed design are presented in Table 15 below.

Case	Stage 1 Flow (kg/s)	Bed Volume (m <sup>3</sup> )	Bed Length (m)	Bed Diameter (m)	Superficial Velocity (m/s)
G/H	3.47	2.76	1.29	1.65	0.357

**Table 15: Bed proportions for cases G and H**

An illustration of the process is shown in Figure 15 below. Note that the purge and process streams should occupy different manifold systems. Only one manifold system is shown in the figure for simplicity. In addition, only a few beds are shown. The modular design of the process allows for installation of more capacity should process requirements change, and the process diagram reflects that consideration. However, if this process is to become feasible, an innovative heating and especially cooling mechanism should be devised in order to reduce regeneration cycle time and thereby the number of beds required.



**Figure 15: Adsorptive separation process diagram**



## Chapter 4: Conclusions and Future Work

### Conclusions of Chromatography, Capacity, and Capacity Loss Experiments

Several conclusions can be drawn from this work. First, this work agrees with the conclusions of prior work in that *m*-cresol adsorbs strongly onto activated carbon while acetic acid adsorbs only weakly, and this difference in adsorptive behavior can be exploited for the purposes of biofuels separations. Second, this work has shown that although acetic acid desorbs almost completely from activated carbon at 250 °C, it remains on the surface long enough to compete for sites with *m*-cresol. Third, this work provides evidence for the hypothesis that a wide variety of adsorption sites exist on the surface of activated carbon, and that adsorption onto those sites varies broadly in both adsorption enthalpy and in adsorptive capacity. This work suggests that there exist multiple mechanisms for the adsorption of phenolic compounds onto activated carbon: hydrogen bonding, for oxygenated sites, and  $\pi$ - $\pi$  stacking, for flat carbon sites; and that certain sites may coordinate both hydrogen bonding and  $\pi$ -interactions for the adsorption of phenolic compounds, such as quinone sites. Fourth, this work shows that at temperatures of interest for biofuels separations, *m*-cresol adsorbs readily onto activated carbon, and is not readily removed, leading to a characteristic breakthrough curve. This breakthrough curve should persist in a scaled-up system for separating biomass thermal degradation product mixtures, and should aid the design of such a system. Fifth, this work designs such a system, entailing a number of adsorption beds which are depleted and regenerated in turn, sized to accommodate a torrefaction process which takes in 2000 tonnes of raw biomass per day.

## Future Work

The work documented here is by no means complete. Several areas of future study could contribute to the interpretation of the results presented here. As described above, a method for studying the effects of column length on chromatographic separation should be devised which does not suffer from the shortcomings of this work: different carrier gas flow rates and asymmetric bed packing. If a column could be constructed which is longer, rather than shorter, than the standard column, it should be possible to conduct experiments on column length. It is suggested that the column should be packed completely, and that the length of stainless steel tubing be the adjustable parameter. This would eliminate the potential confounding effects of empty space at the entrance of the tubing. However, the increased amount of packing may cause an unintended increase in the axial dispersion of some components, resulting in broader, flatter peaks. Because the FID signal-to-noise ratio decreases for broader, flatter peaks, this would introduce more error into peak area results.

Another area of future study should investigate the effects of carbon age on the composition of the surface, and how that affects the adsorptive properties of the carbon. This work suggested that the composition of the surface could change over time, with some oxygenated groups decaying into more stable groups, which have different adsorptive properties than the original groups. Future study on the stability of the oxygenated sites on activated carbon should also consider the potential effect of long temperature exposure on the surface structure. During this work, very small amounts of material were observed volatilizing from fresh carbons, regardless of age, during the isothermal temperature portions of the

TGA/DSC experiments. Although this could be due to residual water adsorbed onto the carbon, its identity could not be confirmed in this work.

Future work could also investigate the adsorptive properties of toluene onto activated carbon more closely. This work recorded a surprisingly high equilibrium adsorption capacity for toluene on activated carbon, which was significantly higher than that of benzene. If benzene and toluene adsorb differently, the mechanism of their adsorption should be studied. It may be that benzene adsorbs via  $\pi$ -interaction using an edge, instead of flat onto the carbon surface. If this is the case in general for aromatic rings, then the methyl group on toluene could increase the barrier to adsorption because it eliminates two potential edges compared to benzene. This would also have implications for the adsorption of *m*-cresol. However, since the adsorption capacity for *m*-cresol was even higher than toluene, it is not likely that edge-on adsorption via  $\pi$ -interaction is the primary mode of adsorption for *m*-cresol.

Lastly, future work should confirm that no reaction between adsorbates occurs on the activated carbon surface. Activated carbon has been shown to promote oxidation and dehydrogenation reactions, and it is possible that adsorbate-adsorbate interactions go further than merely altering adsorptive properties [31, 32]. In order to study the possible catalytic activity of activated carbon for biofuels mixtures, it is suggested to pack the carbon into a Parr reactor with an in-line mass spectrometer. One possible reaction is esterification, with the cresol acting as the alcohol and the acetic acid acting as the acid. The carbon's role in this reaction would likely be an entropic coordination effect, although acidic surface sites such as carboxylic and phenolic groups could also contribute by changing the reaction mechanism. Another possible reaction is oligomerization, with cresol combining via one of several linkages

which hold together monolignol units in natural lignin. The most likely linkage to be formed by cresol is an  $\alpha$ -O-3 or  $\alpha$ -O-4 linkage, depending on whether the cresol is of the meta- or para-isomer, respectively. Although  $\beta$ -O-4 linkages are much more commonly found in natural lignin, cresol does not have an equivalent to the  $\beta$  position. Because heat treatment of used carbon samples at 500 °C released volatile compounds, identifying those compounds via mass spectrometry would be a useful first step in determining whether the activated carbon catalyzes reactions between adsorbates.

## References

1. Central Intelligence Agency, *CIA World Factbook*, Central Intelligence Agency, 2017. [Online]. Available: <https://www.cia.gov/library/publications/the-world-factbook/geos/xx.html> [Accessed: 25 Nov. 2018]
2. P. A. Kharecha and J. E. Hansen, "Implications of 'peak oil' for atmospheric CO<sub>2</sub> and climate," *Global Biogeochemical Cycles*, vol. 22, no. 3, Aug. 2008
3. J. G. Canadell et al., "Contributions to accelerating atmospheric CO<sub>2</sub> growth from economic activity, carbon intensity, and efficiency of natural sinks," *PNAS*, vol. 104, no. 47, Nov. 2007, pp. 18866-18870
4. S. Manabe and R. T. Wetherald, "On the Distribution of Climate Change Resulting from an Increase in CO<sub>2</sub> Content of the Atmosphere," *J. Amer. Met. Soc.*, Jan. 1980
5. M. Eby, K. Zickfeld, and A. Montenegro, "Lifetime of Anthropogenic Climate Change: Millennial Time Scales of Potential CO<sub>2</sub> and Surface Temperature Perturbations," *J. Amer. Met. Soc.*, May 2009
6. C. Rosenzweig and M. L. Parry, "Potential impact of climate change on world food supply," *Nature*, vol. 367, Jan. 1994
7. J. Schmidhuber and F. N. Tubiello, "Global food security under climate change," *PNAS*, vol. 104, no. 50, Dec. 2007, pp. 19703-19708
8. N. E. Heller and E. S. Zavaleta, "Biodiversity management in the face of climate change: A review of 22 years of recommendations," *Biol. Cons.*, vol. 142, no. 1, Jan. 2009, pp. 14-32
9. C. Bellard et al., "Impacts of climate change on the future of biodiversity," *Ecology Letters*, vol. 15, no. 4, Jan. 2012, pp. 365-377
10. A. J. McMichael, R. E. Woodruff, and S. Hales, "Climate change and human health: present and future risks," *The Lancet*, vol. 367, no. 9513, Mar. 2006, pp. 859-869
11. J. A. Patz et al., "Impact of regional climate change on human health," *Nature*, vol. 438, Nov. 2005, pp. 310-317
12. J. R. Regalbuto, "Cellulosic Biofuels – Got Gasoline?" *Science*, vol. 325, no. 5942, Aug. 2009, pp. 822-824
13. C. C. Pereira and V. M. D. Pasa, "Effect of Alcohol and Copper Content on the Stability of Automotive Gasoline," *Energy & Fuels*, vol. 19, no. 2, Jan. 2005, pp. 426-432
14. H. Chen, "Chemical Composition and Structure of Natural Lignocellulose," in *Biotechnology of Lignocellulose: Theory and Practice*, Beijing, Springer, 2014
15. P. J. de Wild, H. Reith, and H. J. Heeres, "Biomass pyrolysis for chemicals," *Biofuels*, vol. 2, no. 2, Jan. 2011, pp. 185-208
16. E. Rich, unpublished
17. G. G. Zaines et al., "Multistage torrefaction and *in situ* catalytic upgrading to hydrocarbon biofuels: analysis of life cycle energy use and greenhouse gas emissions," *Energy & Envir. Sci.*, vol. 10, no. 5, Apr. 2017, pp. 1034-1050
18. D. E. Resasco and S. P. Crossley, "Implementation of concepts derived from model compound studies in the separation and conversion of bio-oil to fuel," *Catalysis Today*, vol. 257, no. 2, Nov. 2015, pp. 185-199

19. P. S. Rezaei, H. Shafaghat, and W. M. A. W. Daud, "Suppression of coke formation and enhancement of aromatic hydrocarbon production in catalytic fast pyrolysis of cellulose over different zeolites: effects of pore structure and acidity," *RSC Advances*, vol. 5, no. 80, Jul. 2015, pp. 65408-65414
20. S. Du, J. A. Valla, and G. M. Bollas, "Characteristics and origin of char and coke from fast and slow, catalytic and thermal pyrolysis of biomass and relevant model compounds," *Green Chem.*, vol. 15, no. 11, Sep. 2013, pp. 3214-3229
21. W. Luo et al., "Ruthenium-catalyzed hydrogenation of levulinic acid: Influence of the support and solvent on catalyst selectivity and stability," *J. Cat.*, vol. 301, May 2013, pp. 175-186
22. A. Dabrowski et al., "Adsorption of phenolic compounds by activated carbon – a critical review," *Chemosphere*, vol. 58, no. 8, Feb. 2005, pp. 1049-1070
23. M. Goyal and R. C. Bansal, "Activated Carbon and its Surface Structure," in *Activated Carbon Adsorption*, New Delhi, Taylor & Francis, May 2014
24. R. E. Franklin and J. D. Watt, "Changes in the structure of carbon during oxidation," *Nature*, vol. 180, 1957, pp. 1190-1191
25. G. S. Szymanski et al., "The effect of the gradual thermal decomposition of surface oxygen species on the chemical and catalytic properties of oxidized activated carbon," *Carbon*, vol. 40, no. 14, 2002, pp. 2627-2639
26. I. Schneberger, "Adsorptive Trapping of Bio-oil Compounds onto Activated Carbon," *ShareOK*, 2016
27. Desotec, "Carbonology," *Desotec*, 2018. [Online]. Available: <https://www.desotec.com/en/carbonology/carbonology-academy/activated-carbon-density> [Accessed: 25 Nov. 2018]
28. X Zhu et al., "Tailoring the mesopore structure of HZSM-5 to control product distribution in the conversion of propanal," *J. Cat.*, vol. 271, Mar. 2010, pp. 88-98
29. J. G. Tittensor, R. J. Gorte, and D. M. Chapman, "Isopropylamine adsorption for the characterization of acid sites in silica-alumina catalysts," *J. Cat.*, vol. 138, no. 2, Dec. 1992, pp. 714-720
30. N. Chada et al., "Activated carbon monoliths for methane storage," *Bull. APS*, vol. 57, no. 1, Mar. 2012
31. F. Lucking et al., "Iron powder, graphite and activated carbon as catalysts for the oxidation of 4-chlorophenol with hydrogen peroxide in aqueous solution," *Water Res.*, vol. 32, no. 9, Sep. 1998, pp. 2607-2614
32. M. F. R. Pereira, J. J. M. Orfao, and J. L. Figueiredo, "Oxidative dehydrogenation of ethylbenzene on activated carbon catalysts. I. Influence of surface chemical groups," *Appl. Cat. A: Gen.*, vol. 184, no. 1, Aug. 1999, pp. 153-160